

Acoustic peaks and dips in the CMB power spectrum: observational data and cosmological constraints

R. Durrer¹

School of Natural Sciences, Institute for Advanced Study, Einstein Drive, Princeton, NJ 08540

B. Novosyadlyj² and S. Apuneych

*Astronomical Observatory of Ivan Franko L'viv National University, Kyryla and Mephodia str.8,
79005, L'viv, Ukraine*

ABSTRACT

The locations and amplitudes of three acoustic peaks and two dips in the Boomerang, MAXIMA and DASI measurements of the cosmic microwave background (CMB) anisotropy power spectra as well as their statistical confidence levels are determined in a model-independent way. It is shown that the Boomerang-2001 data (Netterfield et al. 2001) fixes the location and amplitude of the first acoustic peak at more than 3σ confidence. The next two peaks and dips are determined at a confidence level above 1σ but below 2σ . The locations and amplitudes of the first three peaks and two dips are $\ell_{p_1} = 212 \pm 17$, $A_{p_1} = 5426 \pm 1218 \mu K^2$, $\ell_{d_1} = 413 \pm 50$, $A_{d_1} = 1960 \pm 503 \mu K^2$, $\ell_{p_2} = 544 \pm 56$, $A_{p_2} = 2266 \pm 607 \mu K^2$, $\ell_{d_2} = 746 \pm 89$, $A_{d_2} = 1605 \pm 650 \mu K^2$, $\ell_{p_3} = 843 \pm 35$, $A_{p_3} = 2077 \pm 876 \mu K^2$ respectively (1σ errors include statistical and systematic errors). The MAXIMA and DASI experiments give similar values for the extrema which they determine. For MAXIMA these are the 1st and 3rd peaks, for DASI the 1st and 2nd peaks and the 1st dip. Moreover, the locations and amplitudes of the extrema determined from the combined data of all experiments are quite close to the corresponding values extracted from the Boomerang data alone.

In order to use these data in a fast search for cosmological parameters an accurate analytic approximation to calculate CMB peak and dip positions and amplitudes in mixed dark matter models with cosmological constant and curvature is derived and tested.

The determined cosmological parameters from the CMB acoustic extrema data show good agreement with other determinations, especially with the baryon content as deduced from standard nucleosynthesis constraints (Burles et al. 2001). These data supplemented by constraints from direct measurements of some cosmological parameters

¹Department de Physique Théorique, Université de Genève, Quai Ernest Ansermet 24, CH-1211 Genève 4, Switzerland

²on leave from Department de Physique Théorique, Université de Genève, Switzerland

and data on large scale structure (LSS) lead to a best-fit model which agrees with practically all the used experimental data within 1σ . The best-fit parameters are: $\Omega_\Lambda = 0.64^{+0.14}_{-0.27}$, $\Omega_m = 0.36^{+0.21}_{-0.11}$, $\Omega_b = 0.047^{+0.093}_{-0.024}$, $n_s = 1.0^{+0.59}_{-0.17}$, $h = 0.65^{+0.35}_{-0.27}$ and $\tau_c = 0.15^{+0.95}_{-0.15}$. The best-fit values of Ω_ν and T/S are close to zero, their 1σ upper limits are 0.17 and 1.7 respectively.

Subject headings: cosmology: microwave background anisotropies – acoustic peaks – cosmological parameters

1. Introduction

The new data on the cosmic microwave background (CMB) temperature anisotropy obtained in the Boomerang (de Bernardis et al. 2000; Netterfield et al. 2001), Maxima I (Hanany et al. 2000; Lee et al. 2001) and DASI (Halverson et al. 2001) experiments provide relatively accurate measurements of the CMB anisotropies up to $\ell \sim 1000$. Boomerang is a long duration balloon (LDB) flight around the South Pole, MAXIMA is a balloon flight from Palestine, Texas, and DASI is an interferometer experiment. The mutual agreement of such divers experiments within statistical uncertainties is very reassuring.

After a correction of the first results from Boomerang (de Bernardis et al. 2000) by Netterfield et al. (2001), these measurements are in astounding agreement with the simplest flat adiabatic purely scalar model of structure formation. The best fit cosmological parameters obtained coincide with other, completely independent determinations, like *e.g.* the baryon density parameter predicted by nucleosynthesis (Burles et al. 2001).

CMB anisotropies can be calculated within linear perturbation theory in a multi-component universe. These calculations are very well established and allow accurate predictions of the CMB power spectrum for a given model of initial perturbations and given cosmological parameters. All the calculations are linear and very well controlled. Publicly available codes, *e.g.* CMBfast (Seljak & Zaldarriaga 1996) provide 1% accurate results for a given model within two minutes of CPU time on an ordinary PC. Due to these advantages, CMB temperature fluctuation data are extremely valuable for testing theoretical models of structure formation and for the determination of cosmological parameters.

Nevertheless, the efficiency of parameter determination using codes like CMBfast to compute the temperature anisotropy spectrum for each model has several problems: 1) The complete set of observational data of the current state and the early history of the Universe is described by models with at least six parameters. The implementation of CMBfast-like codes into search procedures for best fits in high dimensional parameter spaces consumes too much CPU time even for the most advanced computers due to the necessity to carry out numerical integration of the Einstein-Boltzmann system of equations which describe the evolution of temperature and density perturbations of each

component through the decoupling epoch. 2) The CMB power spectrum alone has several more or less exact degeneracies in parameter space (see *e.g.* Efstathiou & Bond (1999)) which can only be reduced substantially or removed completely if other data sets, *e.g.* galaxy clustering data, corresponding to different scales and redshifts, are combined with CMB measurements. The results and especially the error bars which are obtained from search procedures using different classes of cosmological observations with different quality and different statistical properties are difficult to interpret.

Several groups have overcome the first problem by computing a grid of CMB anisotropy spectra in the space of models and interpolating between them to obtain the spectra for intermediate values of the parameters (see Tegmark et al. (2001); Lange et al. (2001); Balbi et al. (2000); de Bernardis et al. (2001); Wang et al. (2001) and references therein).

Here we propose an alternative method: The CMB angular power spectrum obtained by COBE (Smoot et al. 1992), Boomerang, MAXIMA-1 and DASI has well defined statistical and systematic errors in the range of scales from quadrupole up to the spherical harmonic $\ell \sim 1000$ and the present data can be represented by a few dozen uncorrelated measurements. Practically the same information is contained in a few characteristics such as the amplitude and inclination of the power spectrum at COBE scale and the amplitudes and locations of the observed acoustic peaks and dips. Indeed, it was shown (see (Hu & Sugiyama 1995; Hu & White 1996; Efstathiou & Bond 1999; Doran & Lilley 2001) and references therein) that the sensitivity of the locations and amplitudes of the extrema, especially of the peaks, to cosmological parameters is the same as their sensitivity to the flat band powers, the C_l 's, from presently available data. This is not surprising: the extrema have an obvious physical interpretation and have the largest weight among data points on CMB power spectrum as a result of a minimal ratio of error to value. Hu et al. (2001) have shown that most of the information from the Boomerang and MAXIMA-1 data sets can be compressed into four observables: amplitude and location of 1-st peak, and amplitudes of 2-nd and 3-rd peak.

The first three acoustic peaks and the two dips indicated by the above mentioned experiments and the COBE large scale data can be presented by not more than 12 experimental points. If we use the approach by Bunn & White (1997) for the four year COBE data and the data on acoustic peaks, we have 7 experimental values to compare with theoretical models. Each of them can be calculated by analytical or semi-analytical methods. This enables us to study present CMB data in a very fast search procedure for multicomponent models.

Even though, in principle, a measurement of the entire C_ℓ spectrum contains of course more informations than the position and amplitudes of its peaks and dips, with present errorbars, this additional informations seems to be quite modest.

The goal of this paper is to use these main characteristics of the CMB power spectrum to determine cosmological parameters. To do this we have to accomplish the following steps: 1) to locate the positions and amplitudes of three peaks and two dips as well as determining their error bars from experimental data, 2) to derive accurate analytical approximations to calculate

these positions and amplitudes and test them by full numerical calculations. We also derive an accurate and fast semi-analytical method to normalize the power spectrum to the 4-year COBE data. Such analytical approximations have been derived in the past for the matter power spectrum (Eisenstein & Hu 1998; Eisenstein & Hu 1999; 1) and for the Sachs-Wolfe part of the CMB anisotropy spectrum (Kofman & Starobinsky 1985; Apuneyvych & Novosyadlyj 2000). Here we derive an analogous approximation for the acoustic part of the CMB anisotropy spectrum by improving an approximation proposed by Efstathiou & Bond (1999).

The outline of the paper is as follows. In Section 2 we determine the locations and amplitudes of the 1st, 2nd and 3rd acoustic peak as well as 1st and 2nd dip and their confidence levels using the published data on the CMB angular power spectrum from Boomerang (Netterfield et al. 2001), MAXIMA-1 (Lee et al. 2001) and DASI (Halverson et al., 2001). Analytical approximations for the positions and amplitudes of the acoustic peaks and dips are described in Section 3. A new method for an accurate and fast COBE normalization is also presented in this section. Details are given in two Appendices. Our search procedure to determine cosmological parameters along with the discussion of the results is presented in Section 4. In Section 5. we draw conclusions.

2. Peaks and dips in the CMB power spectrum: experimental data

We have to determine the locations and amplitudes of acoustic peaks and dips as well as their uncertainties in the data of the angular power spectrum of CMB temperature fluctuations obtained in the Boomerang (Netterfield et al. 2001), MAXIMA-1 (Lee et al. 2001) and DASI (Halverson et al. 2001). We carry out a model-independent analysis of the peaks and dips in the power spectra for each experiment separately, as well as using all data points jointly.

2.1. Boomerang-2001

A model-independent determination of peak and dip locations and amplitudes in the Boomerang data (Netterfield et al. 2001) has been carried out recently by de Bernardis et al. (2001). Our approach is based on a conceptually somewhat different method, especially in the determination of statistical errors.

At first, mainly for comparison of our results with de Bernardis et al. (2001), we fit the peaks in the Boomerang CMB power spectrum by curves of second order (parabolas) as shown in Fig. 1. The six experimental points ($N_{exp} = 6$) in the range $100 \leq \ell \leq 350$, which trace the first acoustic peak, are well approximated by a three parameter curve ($N_{par} = 3$). Hence, the number of degrees of freedom $N_f = N_{exp} - N_{par}$ for the determination of these parameters is $N_f = 3$. The best-fit parabola has $\chi^2_{min} = 2.6$. Its extremum, located at $\ell_{p_1} = 212$ and $A_{p_1} = 5426 \mu K^2$, is the best-fit location and amplitude of the first acoustic peak. We estimate the statistical error in the following way. Varying the 3 parameters of the fitting curve so that $\chi^2 - \chi^2_{min} \leq 3.53$ the maxima of the

parabolas define the 1σ range of positions and amplitudes of the first acoustic peak in the plane $(\ell, \ell(\ell+1)C_\ell/2\pi)$. The boundary of this region determines the statistical 1σ errors for the location and amplitude of the first acoustic peak. We obtain

$$\ell_{p_1} = 212_{-20}^{+13}, \quad A_{p_1} = 5426_{-539}^{+540} \mu K^2.$$

In Fig. 1 the 1σ , 2σ (the boundary of the region with $\chi^2 - \chi^2_{min} \leq 8.02$) and 3σ ($\chi^2 - \chi^2_{min} \leq 14.2$) contours are shown in the plane $(\ell, \ell(\ell+1)C_\ell/2\pi)$. All contours for the first acoustic peak are closed. This shows that the Boomerang-2001 data prove the existence of a first peak at a confidence level higher than 3σ . The values $\Delta\chi^2 = 3.53, 8.02$ and 14.2 , given by the incomplete Gamma function, $Q(N_f, \Delta\chi^2/2) = 1 - 0.683, 1 - 0.954$ and $1 - 0.9973$, correspond to 68.3% , 94.5% and 99.73% confidence levels respectively for a Gaussian likelihood of $N_f = 3$ degrees of freedom. These levels which depend on N_f and thus on the number of independent data points (which we just took at face value from Netterfield et al. (2001)) define the regions within which the maxima of parabolas leading to the data points lie with a probability $\geq p$, where $p = 0.68, 0.954$ and 0.9973 for 1- , 2- and $3\text{-}\sigma$ contours respectively. The same method for the second peak using the eight experimental points in the range $400 \leq \ell \leq 750$, hence $N_f = 5$, gives

$$\ell_{p_2} = 541_{-102}^{+40}, \quad A_{p_2} = 2225_{-227}^{+231} \mu K^2.$$

For the third peak ($750 \leq \ell \leq 1000$, 6 experimental points, $N_f = 3$) we obtain

$$\ell_{p_3} = 843_{-42}^{+25}, \quad A_{p_3} = 2077_{-412}^{+426} \mu K^2.$$

For the second and third peaks, the 2- and $3\text{-}\sigma$ contours are open as shown in Fig. 1. This means that the Boomerang experiment indicates the 2nd and 3rd acoustic peaks at a confidence level higher than 1- but lower than $2\text{-}\sigma$. This is in disagreement with the result obtained in (de Bernardis et al. 2001). Formally the disagreement consists in the fact that de Bernardis et al. (2001) set $N_f = 2$ for all peaks and dips (see paragraph 3.1.2 of their paper) leading to different values of $\Delta\chi^2$ for the 1- , 2- and $3\text{-}\sigma$ contours. They argue that there are two free parameters, namely the height and the position of the peak. The 'philosophy' of the two approaches is somewhat different: While our contours limit the probability that the given data is measured if the correct theoretical curve has the peak position and amplitude inside the contour, in their approach the contours limit the probability that the given best fit parabola leads to data with peak position and amplitude inside the contour. In other words, while they compare a given parabola to the best fit curve, we compare it to the data. In that sense we think that the closed $2\text{-}\sigma$ contours of de Bernardis et al. (2001) do not prove the existence of the secondary peaks at the $2\text{-}\sigma$ level. Of course our approach has a problem as well: It relies on the data points being independent. If they are not, the number of degrees of freedom should be reduced.

The same procedure can be applied for the amplitudes and positions of the two dips between the peaks.

There is also a slight logical problem in the results presented in Fig. 2 of de Bernardis et al.(2001): If 2nd and 3rd peaks are established at 2σ C.L., then the 2nd dip should be determined at the same C.L.; but even the 1σ contour for the position of the second dip is not closed. Also the position of the first dip is actually fixed by a single data point at $\ell = 450$ as can be seen from Fig. 3 in (de Bernardis et al. 2001). In order to remove these problems we approximate the experimental points in the range $250 \leq \ell \leq 850$ (12 experimental points) by one single fifth order polynomial (6 free parameters). The number of degrees of freedom $N_f = 6$. The best-fit curve with $\chi^2_{min} = 3.26$ is presented in Fig. 2. Its 6 coefficients are $a_0 = 1.13 \cdot 10^5$, $a_1 = -944.7$, $a_2 = 3.106$, $a_3 = -4.92 \cdot 10^{-3}$, $a_4 = 3.75 \cdot 10^{-6}$, $a_5 = -1.099 \cdot 10^{-9}$. This method allows us to determine the locations and amplitudes of both dips and of the second peak by taking into account the relatively prominent raises to the third and especially to the first peak. The local extrema of the polynomial best-fit give the following locations and amplitudes of the 1st and 2nd dip (positive curvature extrema) and the 2nd peak (negative curvature) between them. The 1σ error bars are determined as above:

$$\begin{aligned}\ell_{d_1} &= 413_{-27}^{+54}, \quad A_{d_1} = 1960_{-282}^{+272} \mu K^2, \\ \ell_{p_2} &= 544_{-52}^{+56}, \quad A_{p_2} = 2266_{-274}^{+275} \mu K^2, \\ \ell_{d_2} &= 746_{-63}^{+114}, \quad A_{d_2} = 1605_{-436}^{+373} \mu K^2.\end{aligned}$$

The results discussed here are presented in Table 1 and shown in Figs. 1 and 2. In Fig. 2 also the 1σ ($\Delta\chi^2 = 7.04$), 2σ ($\Delta\chi^2 = 12.8$) and 3σ ($\Delta\chi^2 = 20.1$) confidence contours are shown. The 1σ contours for all peaks and dips are now closed. The 2σ contour for the 2nd peak has a 'corridor' connecting it with the 3rd peak. As we have noted before (see Fig. 1), the 2σ confidence contour for the 3rd peak is also open towards low ℓ . This implies that we can not establish the second peak at 2σ C.L. The probability of its location is spread out over the entire range $450 \leq \ell \leq 920$. Therefore at 2σ C.L. we can not state whether the Boomerang-2001 results indicate a second peak without a third, or third without a second or both. We only can state at 2σ C.L. that there are one or two negative curvature extrema of the function $\ell(\ell+1)C_\ell/2\pi$ situated in the range $450 \leq \ell \leq 920$ with amplitude in the range $1500 \leq \ell(\ell+1)C_\ell/2\pi \leq 2700 \mu K^2$. Furthermore, there is one secondary peak present in this ℓ range at 2σ confidence. Now, the contours for the dips are in logical agreement with the information about the second and third peaks. If at 2σ C.L. the 2nd peak can be at the range of the location of 3rd one, then the 1st dip will move to $\ell \sim 520$. Its 2σ contour is closed since the 3rd peak has a closed 2σ C.L. contour at the high ℓ side. On the contrary, the 2nd dip is open at high ℓ as it disappears when the 'second' peak disappears and the 'third' peak becomes the second. The 3σ contours for the 2nd and 3rd peak as well as for 1st and 2nd dips are open in the direction of high ℓ .

So far we discussed only the statistical errors. The Boomerang LDB measurements have two systematic errors: 20% calibration uncertainty and beam width uncertainty leading to scale-dependent correlated uncertainties in the determination of the power spectrum (Netterfield et al. 2001). The calibration error results in the same relative error for all data points and can be taken

into account easily. The beam width uncertainty which induces an error which becomes larger at higher values of ℓ , needs more care.

We estimate the beam width uncertainty as follows: Using the data of Netterfield et al. (2001) for the 1σ dispersion of the CMB power spectrum due to beam width uncertainty, we have to estimate its effect on determination of peak and dip locations and amplitudes. To take into account the effect of a 1σ overestimated beam width we have lowered the central points of the CMB power spectrum presented in Table 3 of (Netterfield et al. 2001) by multiplying them by the ℓ -dependent factor

$$f_o(\ell) = 1 - 1.1326 \cdot 10^{-4} \ell - 2.72 \cdot 10^{-7} \ell^2.$$

To take into account the effect of a 1σ underestimated beam width we raise the central points of CMB power spectrum all by multiplication with the factor

$$f_u(\ell) = 1 - 6.99 \cdot 10^{-5} \ell + 5.53 \cdot 10^{-7} \ell^2.$$

($f_o(\ell)$ and $f_u(\ell)$ are best fits to the Boomerang-2001 data and are shown in Fig. 3). For both cases we have repeated the peak and dip determination procedure. Best-fit values determined for the central points of CMB power spectrum give us the 1σ errors of the peak/dip characteristics due to beam width uncertainties. The results are presented in Table 1. They show that error bars of all peak and dip *locations* caused by the beam width uncertainty are substantially less than the statistical errors. But they dominate for the *amplitude* of the 3rd peak and are comparable with the statistical error for the amplitudes of the 1st dip, the 2nd peak and the 2nd dip. However, the beam size errors are significantly smaller than statistical errors for the 1st acoustic peak.

Since all sources of errors have different nature and are statistically independent they add in quadrature. The resulting symmetrized total errors are shown in the before last and last columns of Table 1. They are used in the cosmological parameter search procedure described in Section 4.

2.2. Adding DASI and MAXIMA-1 data

We have repeated the determination of peak and dip locations and amplitudes with the data of two other experiments, DASI (Halverson et al. 2001) and MAXIMA-1 (Lee et al. 2001), released simultaneously with Boomerang-2001. Both confirm the main features of the Boomerang CMB power spectrum: a dominant first acoustic peak at $\ell \sim 200$, DASI shows a second peak at $\ell \sim 540$ and MAXIMA-1 exhibits mainly a 'third peak' at $\ell \sim 840$. The results presented in Figs. 4,5 and 6 are quantitative figures of merit for their mutual agreement and/or disagreement. In Fig. 4 the 1, 2 and 3σ contours for the first peak location and amplitude for each experiment as well as the contours for the combined data are presented.

In Fig. 4 one sees that MAXIMA, like Boomerang, indicates on the existence of the first acoustic peak at approximately 3σ C.L. But its 1σ contour for location of this peak in the $(\ell, \ell(\ell+1)C_\ell/2\pi)$ plane does not intersect the Boomerang 1σ contour, though their projections on ℓ and $\ell(\ell+1)C_\ell/2\pi$

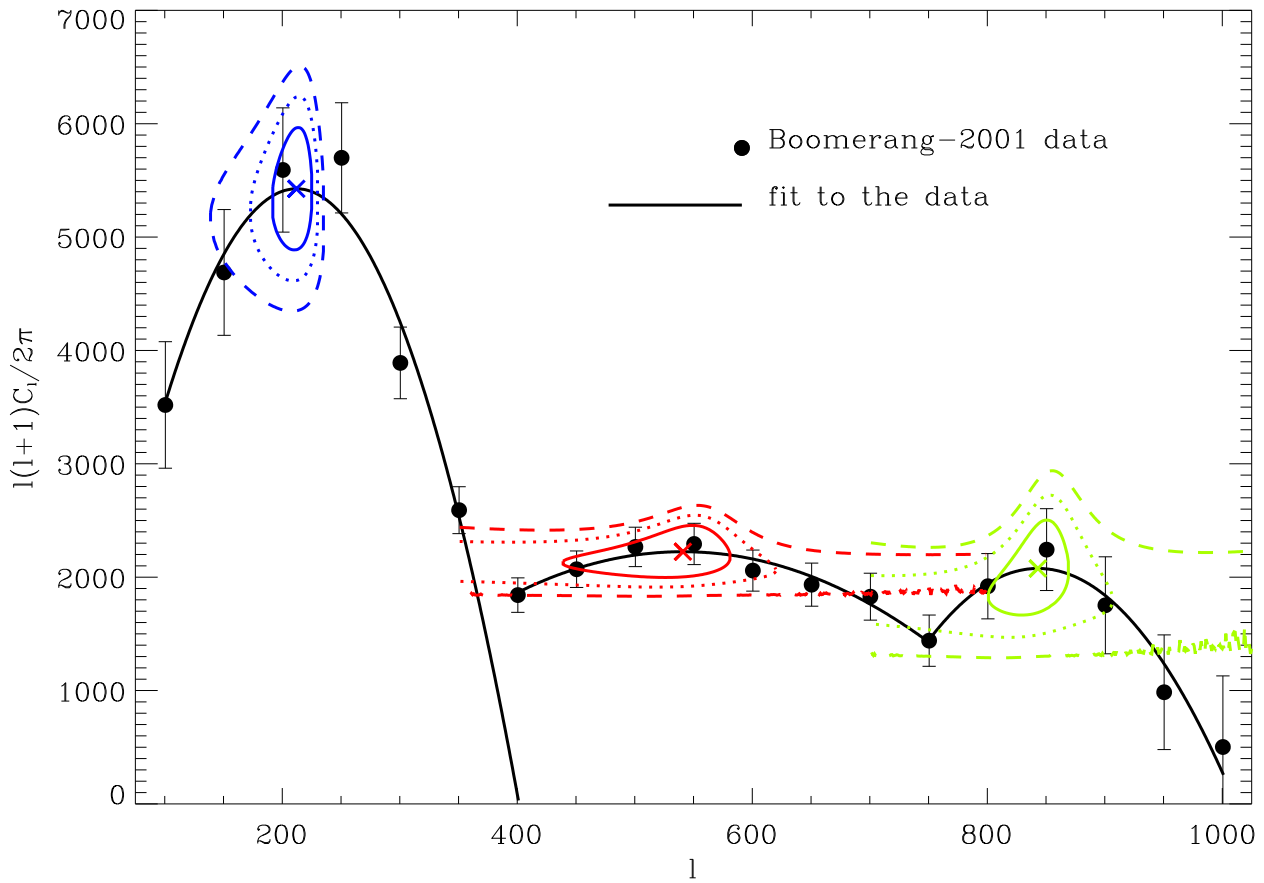


Fig. 1.— Best-fit parabolas for the acoustic peaks of the Boomerang-2001 CMB power spectrum ($\chi^2_{min} = 2.59$ for the 1st peak, $\chi^2_{min} = 0.92$ for the 2nd peak and $\chi^2_{min} = 0.65$ for the 3rd peak) as well as 1 (solid), 2 (dotted) and 3σ (dashed) contours for their locations and amplitudes are shown. The crosses indicate the top of the best-fit parabolas. The contours limit the regions in the $(\ell, \ell(\ell+1)C_\ell/2\pi)$ plane which contain the tops of parabolas with $\Delta\chi^2 = 3.53, 8.02, 14.2$ for the 1st and 3rd peaks ($N_f = 3$) and $\Delta\chi^2 = 5.89, 11.3, 18.2$ for the 2nd peak ($N_f = 5$).

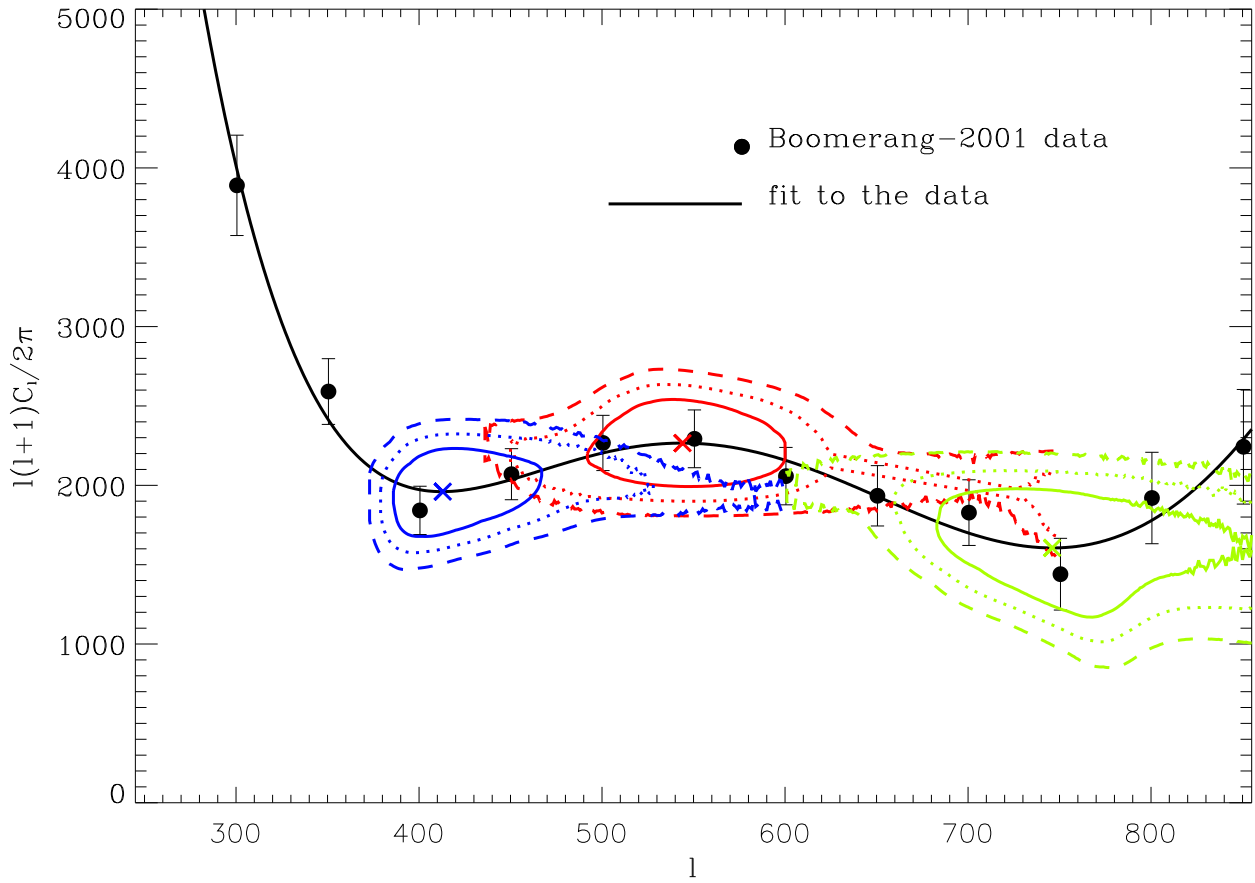


Fig. 2.— The best polynomial fit for the Boomerang-2001 CMB power spectrum in the range of the 1st dip, 2nd peak and 2nd dip ($\chi^2_{min} = 3.26$), and the 1, 2 and 3σ contours for their locations and amplitudes. The crosses indicate the positive (dips) and negative (peak) curvature extrema. The contours limit the regions in the $(\ell, \ell(\ell+1)C_\ell/2\pi)$ plane containing the corresponding extrema of polynomial fits with $\Delta\chi^2 = 7.04, 12.8, 20.1$ ($N_f = 6$).

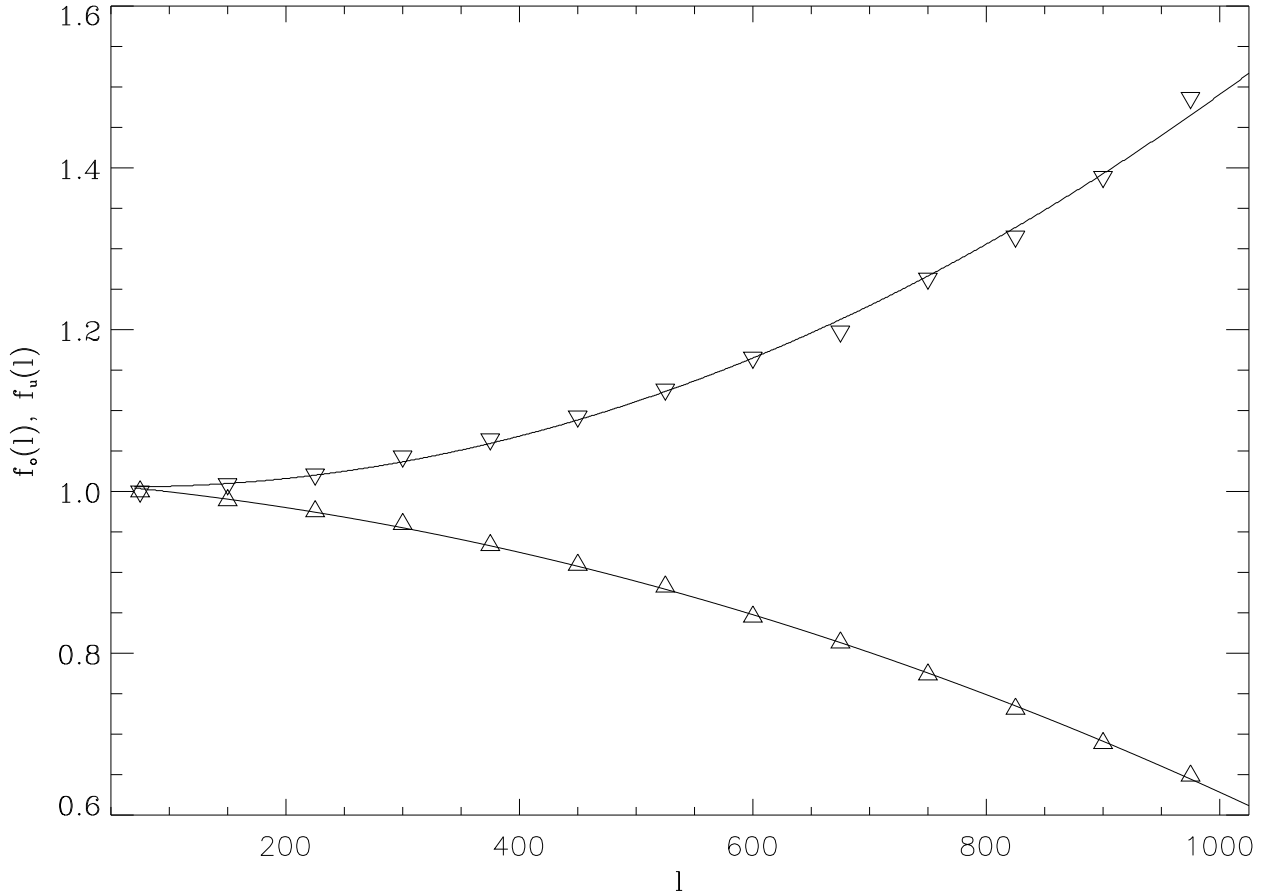


Fig. 3.— The correction factors $f_o(\ell)$ (upward pointing triangles) and $f_u(\ell)$ (downward pointing triangles) for the correlated CMB power spectrum error caused by the uncertainty of the effective beam width of the Boomerang experiment as given in Netterfield et al. (2001). The solid lines are the fitting functions f_o and f_u given in the text.

axes do. This can be caused by systematic (normalization) errors inherent in both experiments. Approximately a quarter of the area outlined by the Boomerang 2σ contour falls within the MAXIMA 2σ contour. The experiments show the same level of agreement in the data on 3rd acoustic peak (Fig. 5). In the range of the 1st dip - 2nd peak - 2nd dip, the MAXIMA data have no significant extrema, even 1σ contours are open in both directions of the ℓ axis.

The DASI experiment establishes the location and amplitude of the first acoustic peak at somewhat more than 1σ but less than 2σ . The remarkable feature is the intersection of the 1σ contours of DASI and Boomerang. Approximately 1/5 of the area outlined by the MAXIMA 2σ contour is within the corresponding DASI contour.

Our analysis has also shown that the DASI data on the second acoustic peak agree very well with Boomerang; the 1σ contours nearly superimpose. The agreement of these two experiments is

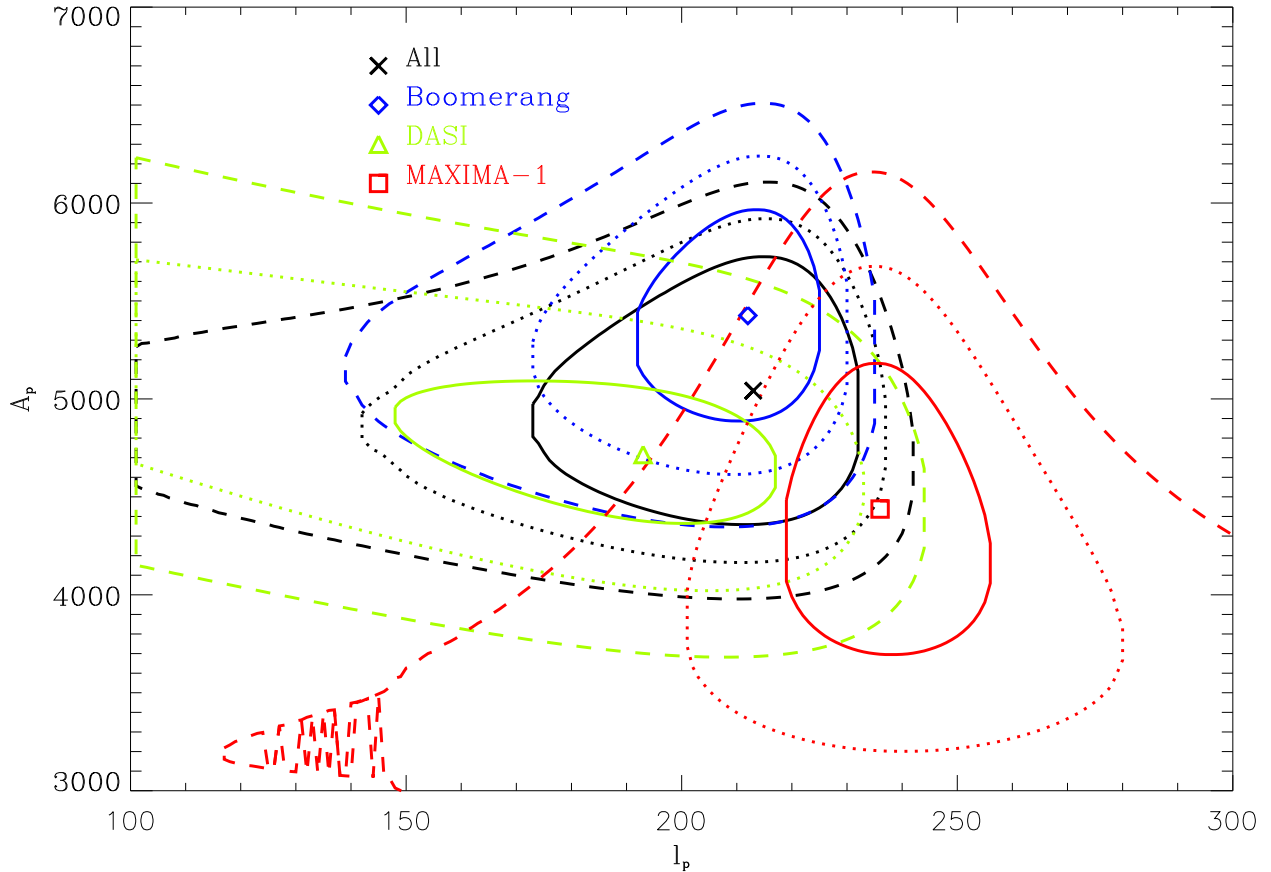


Fig. 4.— The location of the first acoustic peak in the plane $(\ell, \ell(\ell+1)C_\ell/2\pi)$ for the Boomerang-2001 (blue diamond), DASI (green triangle), MAXIMA-1 (red square) data and for all experiments together (black cross) determined as maxima of corresponding best-fit parabola. The 1, 2, 3σ confidence contours are also shown. χ^2_{min} , N_f and $\Delta\chi^2$ for the first peak of the Boomerang-2001 data are given in the caption of Fig. 1, for the other cases we have: DASI – $\chi^2_{min} = 1.8$, $N_f = 1$ and $\Delta\chi^2 = 1, 4, 9$ for the 1, 2, 3σ confidence contours accordingly, MAXIMA-1 – $\chi^2_{min} = 4.22$, $N_f = 2$ and $\Delta\chi^2 = 2.3, 6.17, 11.8$, all experiments together – $\chi^2_{min} = 15.3$, $N_f = 9$ and $\Delta\chi^2 = 10.43, 17.18, 25.26$. The dominant contribution to χ^2_{min} comes from the MAXIMA-1 data.

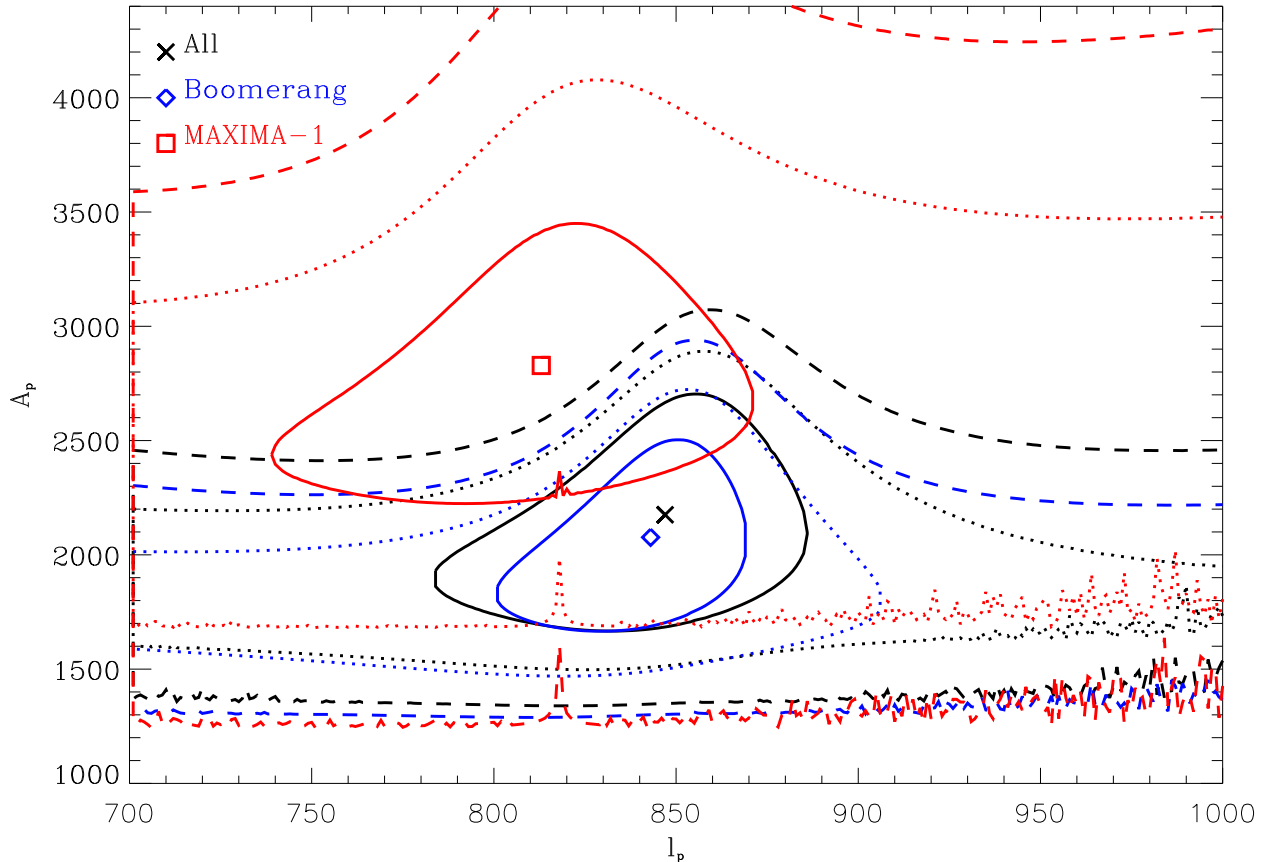


Fig. 5.— The location of the third acoustic peak in the plane $(\ell, \ell(\ell + 1)C_\ell/2\pi)$ for the Boomerang-2001 (blue diamond) and MAXIMA-1 (red square) data and for both experiments together (black cross), determined as maxima of the corresponding best-fit parabola. The 1, 2, 3 σ confidence contours are also shown. χ^2_{min} , N_f and $\Delta\chi^2$ for the Boomerang-2001 third acoustic peak is given in the caption of Fig. 1, for the other cases we have: MAXIMA-1 – $\chi^2_{min} = 0.67$, $N_f = 1$ and $\Delta\chi^2 = 1, 4, 9$, all experiments together – $\chi^2_{min} = 3.0$, $N_f = 6$ and $\Delta\chi^2 = 7.04, 12.82, 20.06$. The dominant contribution to χ^2_{min} comes from the MAXIMA-1 data.

impressive.

We have repeated the determination of peak and dip locations and amplitudes using the data of all experiments jointly. The contours for the combined data are shown by the thicker black lines in Figs. 4 and 5. The C.L. contours for the 1st dip, 2nd peak and 2nd dip determined as regions of locations of negative and positive extrema of a 5-th order polynomial fit are shown in Fig. 6. The comparison with the corresponding figure for the Boomerang data alone (Fig. 2) shows their agreement.

The best-fit values of ℓ_{p_i} , A_{p_i} ($i = 1, 2, 3$) and ℓ_{d_k} , A_{d_k} ($k = 1, 2$) as well as their 1σ statistical errors are given in Table 2.

Other methods of model-independent determinations of acoustic oscillation extrema were proposed by (Douspis & Ferreira 2001; Miller & Nichol 2001). Their analysis like ours finds low statistical significance (less than 2σ) for the detection of second and third peaks.

The peak locations and amplitudes from the Boomerang-2001 CMB data presented in the Table 1 show good quantitative agreement in the locations and, somewhat less good, in the amplitudes obtained from the corresponding data of the other experiments and all the data together. The agreement can be improved when other error sources (calibration, beam width uncertainty, cosmic variance etc) of each experiment are taken into account. With some luck, the new mission MAP, which has been launched successfully last June, will remove many of the current problems and will considerably improve the data on CMB power spectrum.

Clearly, the existence of the first peak in the spectrum is very well established in the present experiments. It has already been established (with less accuracy) before (see, eg. (Knox & Page 2000; Novosyadlyj et al. 2000)). Finally we have also assessed approximately the probability for each of the experiments to show no secondary peaks structure whatsoever. For the Boomerang data this probability is less than 4.6%, while for MAXIMA it is on the order of 15% and for DASI about 8%.

3. Analytic determinations of the locations and amplitudes of the acoustic peaks and dips

In order to use the data in Tables 1 and 2 to determine cosmological parameters, we need a fast algorithm to calculate the peak and dip positions for a given model. Here we improve the analytical approximations of peak/dip positions and amplitudes which have been derived in several papers (Efstathiou & Bond 1999; Hu et al. 2001; Durrer & Novosyadlyj 2001; Doran & Lilley 2001). We start by discussing the normalization procedure.

Table 1. Best fit values for locations (ℓ_p) and amplitudes (A_p , [μK^2]) of the peaks and dips in the CMB temperature fluctuation power spectrum measured by Boomerang (Netterfield et al. 2001). Statistical errors (1st upper/lower values) and errors caused by beam width uncertainties (2nd upper/lower values) are shown in columns 2 and 3. The 20% calibration uncertainty is included in the symmetrized total errors presented in the last column.

Features	ℓ_p	A_p	ℓ_p	A_p
1st peak	212^{+13+2}_{-20-3}	$5426^{+540+112}_{-539-135}$	212 ± 17	5426 ± 1218
1st dip	413^{+54+6}_{-27-6}	$1960^{+272+142}_{-282-158}$	413 ± 50	1960 ± 503
2nd peak	544^{+56+14}_{-52-14}	$2266^{+275+309}_{-274-283}$	544 ± 56	2266 ± 607
2nd dip	746^{+114+9}_{-63-9}	$1605^{+373+422}_{-436-362}$	746 ± 89	1605 ± 650
3rd peak	843^{+26+5}_{-42-7}	$2077^{+426+720}_{-411-573}$	843 ± 35	2077 ± 876

Table 2. Best fit values for the locations and amplitudes of peaks and dips in the CMB temperature fluctuation power spectrum from the DASI and MAXIMA-1 experiments. Statistical errors are determined as described in the text. In the last column the results obtained from the data of all three experiments together are presented.

Features	DASI		MAXIMA-1		All three experiments	
	ℓ_p	A_p	ℓ_p	A_p	ℓ_p	A_p
1st peak	193^{+24}_{-45}	4716^{+376}_{-351}	236^{+20}_{-17}	4438^{+743}_{-743}	213^{+35}_{-59}	5041^{+1017}_{-1196}
1st dip ^a	378^{+15}_{-11}	1578^{+170}_{-178}	475^{+264}_{-83}	1596^{+427}_{-443}	406^{+97}_{-32}	1843^{+385}_{-405}
2nd peak ^a	536^{+30}_{-24}	2362^{+176}_{-176}	$435 - 739^b$	$1500 - 2800^b$	545^{+204}_{-89}	2266^{+397}_{-609}
2nd dip ^a	709^{+45}_{-46}	1799^{+221}_{-308}	$435 - 739^b$	$1000 - 2700^b$	736^{+163}_{-117}	1661^{+517}_{-663}
3rd peak	–	–	813^{+286}_{-112}	2828^{+1880}_{-1584}	847^{+252}_{-146}	2175^{+897}_{-836}

^aThe extrema were determined by approximating the experimental CMB power spectrum by 5-th order polynomial

^bJust the ranges where the probability to find the peak or dip is $> 68.3\%$ are indicated

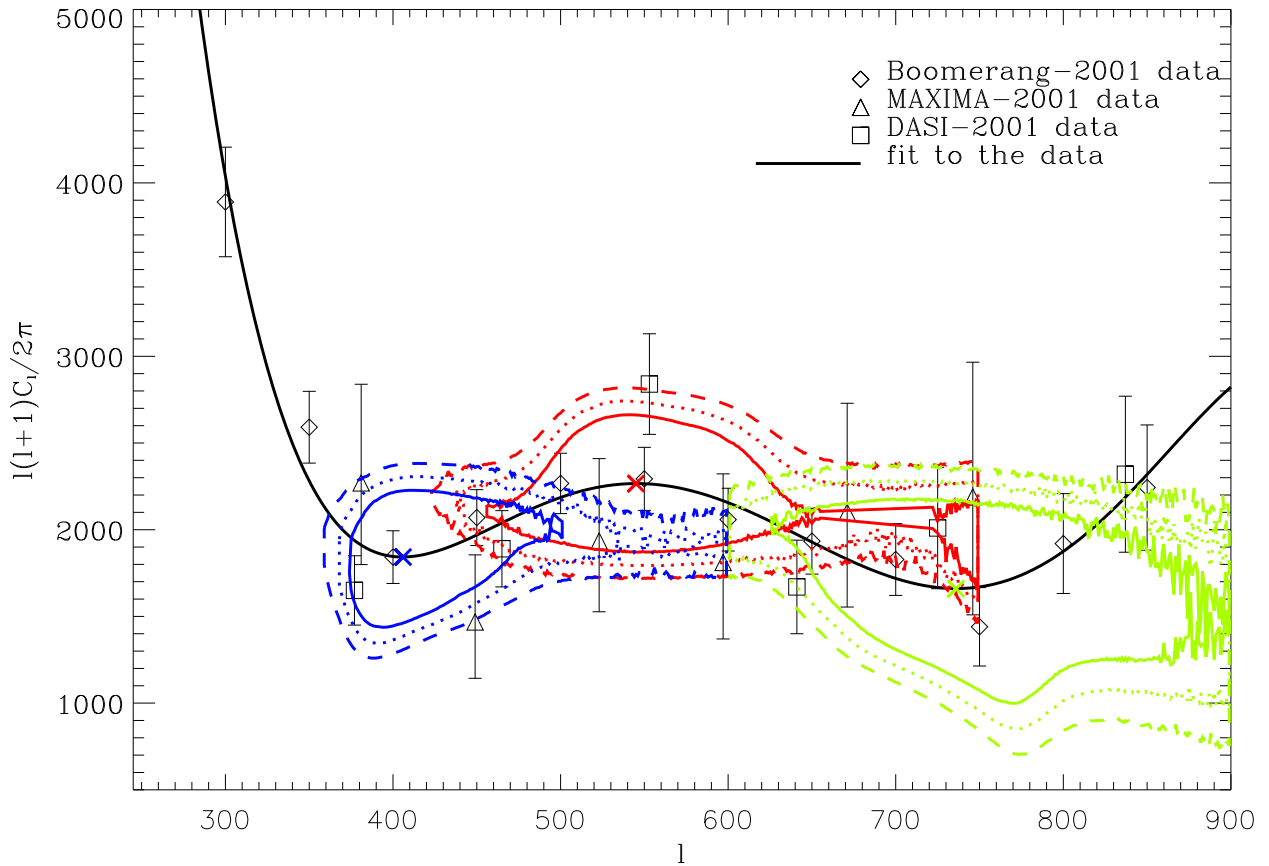


Fig. 6.— The locations of the second acoustic peak and the two dips in the $(\ell, \ell(\ell+1)C_\ell/2\pi)$ plane are shown together with the best-fit 5-th order polynomial. All points in this range from Boomerang, MAXIMA-1 and DASI have been used jointly. The second peak and the dips are determined as extrema of negative and positive curvature of the corresponding best fit polynomial. The $1, 2, 3\sigma$ confidence contours are also shown. For all experiments together, the best-fit gives $\chi^2_{min} = 17.8$ for $N_f = 18$ degrees of freedom.

3.1. Normalization of the density power spectrum

The 4-year COBE data, which establish the amplitude and the form of the CMB power spectrum at the largest angular scales ($\ell \leq 20$), are taken into account via the approximation for C_{10} proposed by Bunn & White (1997). This requires accurate calculations of C_ℓ in the range $\ell \leq 12$. The dominant contribution on these angular scales is given by ordinary Sachs-Wolfe (SW) effect. However, the Doppler (D) effect and the cross-correlation term Sachs-Wolfe – adiabatic (SW-A) in the general expression for the correlation function $\langle \frac{\Delta T}{T}(\mathbf{n}_1) \cdot \frac{\Delta T}{T}(\mathbf{n}_2) \rangle$ have to be taken into account as well if we want to achieve an accuracy better than 20% (see Appendix A). For Λ dark matter models and models with non-zero 3-curvature, also the integrated Sachs-Wolfe effect (ISW) contributes. We use the factors K_ℓ (≥ 1) introduced and calculated by Kofman & Starobinsky (1985) and improved by Apuneych & Novosyadlyj (2000), so that $C_\ell^{\text{SW+ISW}} = K_\ell^2 C_\ell^{\text{SW}}$ (for details see Appendix A).

The normalization of the power spectrum of scalar perturbations then consist in two steps:

- i) We calculate

$$C_\ell = C_\ell^{\text{SW+ISW}} + C_\ell^{\text{D}} + C_\ell^{\text{A}} + C_\ell^{\text{SW-A}} \quad (1)$$

(for $\ell = 2, 3, 5, 7, 10, 11, 12$) by the analytical formulae given in Appendix A with arbitrary normalization. This determines the shape of the CMB power spectrum in the range of the COBE data, and hence the best-fit parameter C_{10}^{COBE} to 4-year COBE and the first and second derivatives as defined in Bunn & White (1997) for models with given cosmological parameters;

ii) Since each term in the expression (1) is $\propto \delta_h^2$, where δ_h is the present matter density perturbations at horizon scale, we can now determine δ_h and along with it the value of the normalization constant for scalar perturbations $A_s = 2\pi^2 \delta_h^2 (3000 \text{Mpc}/h)^{3+n_s}$ for a model with given cosmological parameters. Here n_s is the spectral index for primordial scalar density perturbations and h is dimensionless Hubble parameter (in units of 100 km/sec/Mpc).

Both these steps are also performed in CMBfast. Hence, our normalization procedure for the power spectrum is equivalent to normalization with CMBfast. Calculations show that our value C_{10}^{COBE} never differs from the result of CMBfast by more than 3%. The accuracy of the overall normalization constant δ_h for ADM models with appropriate values of parameters is better then 5%. This has been controlled by comparing the value of σ_8 from CMBfast with our semi-analytical approach. This error simply reflects the accuracy of the analytical approximation of the transfer function for density fluctuations by Eisenstein & Hu (1999) which we have used.

3.2. Positions and amplitudes of CMB extrema: analytic approach

One of the main ingredients for our search procedure is a fast and accurate calculation of the positions and amplitudes of the acoustic peaks and dips, which depend on cosmological parameters.

The dependence of the position and amplitude of the first acoustic peak of the CMB power spectrum on cosmological parameters has been investigated using CMBfast. As expected, the results are, within reasonable accuracy, independent of the hot dark matter contribution (Ω_ν). This was also shown by Novosyadlyj et al. (2000). For the remaining parameters, n_s , h , Ω_b , Ω_{cdm} and Ω_Λ , we determine the resulting values ℓ_{p_1} and A_{p_1} using the analytical approximation given by Efstathiou & Bond (1999) and Durrer & Novosyadlyj (2001). In these papers the CMB anisotropy spectrum is approximated in the vicinity of the first acoustic peak by

$$\frac{\ell(\ell+1)}{2\pi}C_\ell = \frac{\ell(\ell+1)}{2\pi}(C_\ell^{SW} + 0.838C_2^{SW} \cdot \mathcal{A}(\Omega_b, \Omega_{cdm}, \Omega_k, n_s, h) \exp\left[-\frac{(\ell - \ell_{p_1})^2}{2(\Delta\ell_{p_1})^2}\right]), \quad (2)$$

where $\Delta\ell_{p_1} = 0.42\ell_{p_1}$, C_ℓ^{SW} is the Sachs-Wolfe approximation for the C_ℓ s derived in the Appendix A, Eq. (A9), and

$$\begin{aligned} \mathcal{A}(\Omega_b, \Omega_{cdm}, \Omega_k, n_s, h) = & \\ \exp[a_1 + a_2\omega_{cdm}^2 + a_3\omega_{cdm} + a_4\omega_b^2 + a_5\omega_b + & \\ + a_6\omega_b\omega_{cdm} + a_7\omega_k + a_8\omega_k^2 + a_9(n_s - 1)]. & \end{aligned} \quad (3)$$

Here $\omega_b \equiv \Omega_b h^2$, $\omega_{cdm} \equiv \Omega_{cdm} h^2$, $\omega_k \equiv (1 - \Omega_m - \Omega_\Lambda)h^2$. The position of the acoustic peaks is determined as in (Efstathiou & Bond 1999) for open and flat models and in (Durrer & Novosyadlyj 2001) for closed models. The coefficients a_i are defined by fitting to the numerical CMBfast amplitudes of the first acoustic peak on a sufficiently wide grid of parameters. We find: $a_1 = 2.503$, $a_2 = 8.906$, $a_3 = -7.733$, $a_4 = -115.6$, $a_5 = 35.66$, $a_6 = -7.225$, $a_7 = 1.96$, $a_8 = -11.16$, $a_9 = 4.439$. The accuracy of the approximation is better than 5% in the parameter range $0.2 \leq \Omega_m \leq 1.2$, $0 \leq \Omega_\Lambda \leq 0.8$, $0.015 \leq \Omega_b \leq 0.12$, $0.8 \leq n_s \leq 1.2$ and $0.4 \leq h \leq 1.0$. The approximation for the amplitude breaks down in the models with large curvature ($\Omega_k \leq -0.2$ and $\Omega_k \geq 0.6$) and low baryon density, ($\omega_b \ll 0.006$).

To calculate the amplitudes of the 2nd and 3rd peaks, we use the analytic relations for the relative heights of these peaks w.r.t the first peak as given by Hu et al. (2001).

$$\begin{aligned} A_{p_2} &= A_{p_1} H_2(\Omega_m, \Omega_b, n_s), \\ A_{p_3} &= A_{p_1} H_3(\Omega_m, \Omega_b, n_s), \end{aligned} \quad (4)$$

where the functions H_2 and H_3 are given in Eqs. (B16) and (B17) respectively. For the locations of 2nd and 3rd peaks we use the analytic approximations given by Hu et al. (2001) and Doran & Lilley (2001) (see also Appendix B).

Unfortunately, we have no analytic approximation for the dip amplitudes and hence we can not use their experimental values to determine cosmological parameters. But a sufficiently accurate analytic approximation for the location of the 1st dip is given in Doran & Lilley (2001). We use it here.

Hence, we have analytical approximations for the dependences of the positions and amplitudes of three acoustic peaks and the location of the 1st dip on cosmological parameters

$$\begin{aligned} & \ell_{p_i}(\Omega_m, \Omega_\Lambda, \Omega_k, \Omega_b, h), \\ & A_{p_i}(\Omega_m, \Omega_\Lambda, \Omega_k, \Omega_b, n_s, h), \quad (i = 1, 2, 3) \\ & \ell_{d_1}(\Omega_m, \Omega_\Lambda, \Omega_k, \Omega_b, h). \end{aligned}$$

Comparing the analytical values for different sets of parameters with numerical calculations using CMBfast, shows that the accuracy is about 5% for all locations and amplitudes of 1st and 3rd peaks in the ranges of cosmological parameters indicated above. The accuracy for amplitude of the 2nd peak is always better than 9% in the same ranges. For some parameter values the second peak is underestimated.

Of course, in principle the half-widths of peaks and dips, their "smoothness", "sharpness" or their inflection points may contain additional information on cosmological parameters. But when one compares CMB spectra obtained in the different experiments up to date, one concludes that their accuracy is not sufficient to influence the resulting cosmological parameters at the present precision. Therefore, we only use the most prominent observable patterns of the CMB power spectrum - locations and amplitudes of acoustic peaks.

For the convenience, we present all analytic approximations used here in Appendix B.

4. Cosmological parameters from the CMB peak amplitudes and locations

We now use the results of Sections 2 and 3 to determine the cosmological parameters Ω_m , Ω_Λ , Ω_ν (one sort of massive neutrino), Ω_b , n_s , h , T/S ($\equiv C_{10}^{\text{tensor}}/C_{10}^{\text{scalar}}$) and τ_c (optical depth to decoupling). We use the method described in detail in a previous paper (Durrer & Novosyadlyj 2001). We include 8 experimental points from the CMB power spectrum (COBE C_{10} , the amplitudes and locations of three acoustic peaks and the location of the first dip). In order to have a positive number of degrees of freedom, $N_f \geq 1$ we add a weak constraint for the Hubble constant, $0.5 \leq h \leq 0.8$ when searching for 8 parameters.

In order to establish 1σ confidence intervals for each parameter we have applied the marginalization procedure described in (Durrer & Novosyadlyj 2001). The results are presented in Table 3.

At first we check how the best fit parameters depend on the accuracy of the peak/dip locations and amplitudes. For this we compare the resulting cosmological parameters from the data given in Table 1 if we consider only statistical errors and with total errors. The results are given in the first two rows of Table 3. In spite of the different errors of the experimental values and their relations (the total errors of peak amplitudes increase faster with the peak number than the statistical error) the best fit cosmological parameters are similar.

In order to estimate the sensitivity of cosmological parameters to experimental values we

substitute the Boomerang data on peak/dip locations and amplitudes by the values from Table 2, obtained from all three experiments combined. The comparison of the results in the third row with those above shows that the results are practically unchanged. We believe that the Boomerang data on peak/dip locations and amplitudes are best studied and have well established statistics, hence we use them in the following determinations.

The neutrino contents for these three data sets can be rather large, $\Omega_\nu \sim 0.3$. This is due to the low sensitivity of the CMB anisotropy spectrum to Ω_ν . When $\Omega_\nu = 0$ is fixed, the best-fit values for the remaining parameters stay practically unchanged and also χ^2 increases only very little. The CMB doesn't care whether dark matter should be hot or cold. In order to distinguish between cold and hot dark matter data which is sensitive to the density power spectrum on smaller scales needs to be added. In Table 3 we therefore exclude Ω_ν from the determination procedure and fix its value to 0 in the first five rows. Contrary, for T/S and τ_c we obtain 0, but with large 1σ confidence limits due to the degeneracy in T/S , τ_c and n_s (Efstathiou & Bond 1999).

A remarkable result is the good agreement of the best-fit content of baryons $\Omega_b h^2 \approx 0.02$ with the constraint from standard nucleosynthesis and the observed intergalactic content of light elements (Burles et al. 2001). The large 1σ confidence limits for Ω_m and Ω_Λ are due to the well known degeneracy of the CMB power spectrum in these parameters (Efstathiou & Bond 1999). However, the sum of their best fit values, $\Omega_m + \Omega_\Lambda = 1 - \Omega_k$ is always very close to 1 which implies that spatial curvature is small for the best fit model.

We repeat the search procedure for different combinations of the CMB power spectrum extrema data (Table 1) with other cosmological data sets. The LSS data set used here ranges from the Lyman alpha forest, determining amplitude and spectral index of the matter power spectrum at very small scales, to large scale bulk velocities, cluster abundances and Abell cluster catalogs which determine σ_8 and the position of the 'knee' in the matter power spectrum. All of this is extensively discussed in (Durrer & Novosyadlyj 2001).

The results for cosmological parameters from different combinations of observational data are shown in the lines 4 to 8 of Table 3.

Adding a stronger constraint on the Hubble parameter, $h = 0.65 \pm 0.10$, and the big bang nucleosynthesis (BBN) constraint changes the best fit cosmological parameters only slightly. The SNIa constraint on the relation between Ω_Λ and Ω_m (Perlmutter et al. 1999) substantially reduces the errors of these parameters (5th line in Table 3) as it removes the degeneracy between them. This degeneracy is also removed when we combine CMB and LSS data.

The cosmological parameters obtained from the Boomerang CMB power spectrum extrema data combined with all other cosmological measurements (a detailed list can be found in Durrer & Novosyadlyj 2001) are presented in lines 6th, 7th and 8th of Table 3. The best fit values for the tensor mode amplitude T/S defined as C_{10}^T/C_{10}^S in the last two cases are practically zero but the 1σ confidence limits are wide due to the degeneracy of the CMB extrema in n_s , T/S and τ_c . Even when combining the CMB with LSS data, the degeneracy in n_s and T/S is not significantly removed.

Table 3. Cosmological parameters from the extrema of the CMB angular power spectrum in combination with other cosmological data sets. The upper/low values show 1σ confidence limits which are obtained by maximizing the (Gaussian) 68 percent confidence contours over all other parameters. The LSS data set is the same as in (Durrer & Novosyadlyj 2001).

Observable data set	χ^2_{min}/N_f	Ω_Λ	Ω_m	Ω_ν	Ω_b	n_s	h	T/S	τ_c
CMB(<i>Boom,stat.</i>)	1.01/2	$0.69^{+0.23}_{-0.56}$	$0.31^{+0.61}_{-0.21}$	0*)	$0.055^{+0.13}_{-0.028}$	$0.89^{+0.81}_{-0.08}$	$0.65^{+0.23}_{-0.24}$	0^{+27}	$0^{+1.65}$
CMB(<i>Boom,total</i>)	0.95/2	$0.64^{+0.31}_{-1.42}$	$0.36^{+1.04}_{-0.35}$	0*)	$0.057^{+0.18}_{-0.047}$	$0.89^{+0.97}_{-0.14}$	$0.65^{+0.23}_{-0.23}$	0^{+44}	$0^{+1.90}$
CMB(<i>All,stat.</i>)	0.09/2	$0.63^{+0.35}_{-1.35}$	$0.37^{+1.04}_{-0.36}$	0*)	$0.051^{+0.29}_{-0.05}$	$0.90^{+1.30}_{-0.11}$	$0.65^{+0.23}_{-0.24}$	0^{+20}	$0^{+1.75}$
CMB(<i>Boom,total</i>) +									
h & BBN ^a	1.11/3	$0.69^{+0.26}_{-1.30}$	$0.31^{+1.05}_{-0.24}$	0*)	$0.047^{+0.048}_{-0.018}$	$0.90^{+0.56}_{-0.10}$	$0.65^{+0.20}_{-0.19}$	$0^{+2.7}$	$0^{+0.90}$
h , BBN & SNIa ^b	1.11/4	$0.72^{+0.17}_{-0.21}$	$0.29^{+0.15}_{-0.13}$	0*)	$0.047^{+0.048}_{-0.02}$	$0.90^{+0.60}_{-0.12}$	$0.65^{+0.22}_{-0.19}$	$0^{+3.5}$	$0^{+1.1}$
h , BBN & LSS ^c	8.22/11	$0.46^{+0.31}_{-0.46}$	$0.48^{+0.52}_{-0.22}$	$0.06^{+0.20}_{-0.06}$	$0.047^{+0.12}_{-0.026}$	$1.03^{+0.59}_{-0.23}$	$0.66^{+0.31}_{-0.31}$	$0^{+3.5}$	$0.15^{+0.95}_{-0.15}$
h , BBN, SNIa & LSS ^d	10.4/12	$0.64^{+0.14}_{-0.27}$	$0.36^{+0.21}_{-0.11}$	$0.00^{+0.17}_{-0.00}$	$0.047^{+0.093}_{-0.024}$	$1.0^{+0.59}_{-0.17}$	$0.65^{+0.35}_{-0.27}$	$0^{+1.7}$	$0.15^{+0.95}_{-0.15}$
the same ^e	11.6/14	$0.61^{+0.16}_{-0.26}$	$0.37^{+0.21}_{-0.13}$	$0.00^{+0.11}_{-0.00}$	$0.041^{+0.043}_{-0.023}$	$0.95^{+0.17}_{-0.14}$	$0.70^{+0.34}_{-0.20}$	0*)	0*)

*) This parameter is fixed to 0.

^aThe big bang nucleosynthesis constraint on baryon content $\widetilde{\Omega_b h^2} = 0.02 \pm 0.001$ from Burles et al. (2001) is included.

^bThe constraint on the $\Omega_\Lambda - \Omega_m$ relation from SNIa distance measurements (Perlmutter et al. 1999), $[\Omega_m - \widetilde{0.75\Omega_\Lambda}] = -0.25 \pm 0.125$ is added.

^cIn addition to the parameters given in the different columns, we have also to determine the Abell-ACO biasing parameter, b_{cl} . The result is: $b_{cl} = 2.64 \pm 0.27$

^dFor this data set we obtain $b_{cl} = 2.47 \pm 0.19$

^e $b_{cl} = 2.5 \pm 0.2$

This is so, since a blue spectrum, which allows for a high tensor contribution to the CMB, can be compensated with a neutrino component which leads to damping of the matter power spectrum on small scales. If massive neutrinos are not allowed, the degeneracy between n_s and T/S is lifted as soon as small scale LSS data is included.

The best-fit values of spectral index n_s in all cases are in the 1σ range of the value obtained from the COBE 4-year data, $n_s = 1.2 \pm 0.3$ (Bennett et al. 1996; Gorski et al. 1996). When using the best fit model to calculate the data used to find it, practically all results are within the 1σ error range of the corresponding experimental data. Only two out of 31 experimental points are slightly outside. Namely the best-fit value of $\Omega_m - 0.75\Omega_\Lambda$ in the last determination is at 1.1σ lower of its experimental value followed from SNIa test and σ_8 constraint established by (Bahcall & Fan 1998) from the existence of three massive clusters of galaxies is at 1.18σ higher than model predicted value. But the value of σ_8 in our best-fit model, $\sigma_8 = 0.91$, is in the range of current estimates from the Sloan Digital Sky Survey $\sigma_8^{(SLOAN)} = 0.915 \pm 0.06$, (SDSS Collaboration 2001)), which is not included in our data set. The high degree of consistency within completely independent cosmological data sets is very encouraging.

Moreover, all parameters of our best-fit model agree well with those extracted from the full Boomerang data (Netterfield et al. 2001) combined with LSS and SNIa priors (compare our values derived from CMB+LSS in the 7th row of Table 3 and theirs in the 4th row of Table 4). But our 1σ ranges for most parameters are significantly wider. That is due to two facts. First of all, we allow also for a tensor component and neutrinos. This increase in the number of parameters also increases the degeneracies (e.g. between the tensor amplitude and the spectral index n_s) thereby enlarging the errors of the physical parameters. In this sense our parameter errors are rather to be compared with those of Wang et al. (2001) which allow for roughly the same degrees of freedom. But even their parameter estimation is somewhat more precise than ours. This is because we use more conservative errors for the peak and dip locations and amplitudes which include statistical, normalization and beam uncertainties. We think that with present data, and with the model assumptions made by our choice of parameters, our precision is realistic. Clearly, future experiments like the MAP satellite will improve this situation.

Finally, to compare with the cosmological parameters obtained in our previous paper (Durrer & Novosyadlyj 2001, Table 4), where the same LSS data set was used, we have repeated the search procedure fixing $T/S = \tau_c = 0$. The best-fit values of the parameters with 1σ errors obtained by maximizing the confidence contours over all other parameters are given in the last row of Table 3. Comparing them with values in the last column of Table 4 from (Durrer & Novosyadlyj 2001) shows that both determinations have best-fit values in the 1σ confidence limits of each other. There the best fit model has a slight positive curvature, here a slightly negative. The 1σ confidence ranges here are somewhat wider than those obtained in the previous determination. These differences are due to the different CMB observable data set and the different normalization procedure. Even though in our previous analysis we have only taken into account the first peak. The errors in its location and amplitude were significantly underestimated, leading to smaller error bars.

5. Conclusions

We have carried out a model-independent analysis of recent CMB power spectrum measurements in the Boomerang (Netterfield et al. 2001), DASI (Halverson et al. 2001) and MAXIMA (Lee et al. 2001) experiments and we have determined the locations and amplitudes of the first three acoustic peaks and two dips as well as their confidential levels (Table 1-2, Fig. 1-7).

In the Boomerang experiment the second and third acoustic peaks are determined at a confidence level somewhat higher than 1σ . Experimental errors which include statistics and systematics are still too large to establish the secondary peak locations and amplitudes at 2σ C.L. Only the position of one (the third) secondary peak can be bounded from above $\ell_{p_3} \leq 900$, at 2σ C.L. The same situation is encountered when determining the locations and amplitudes of the first and second dips. However, the location and amplitude of the first peak, are well established with confidence level, higher than 3σ .

The MAXIMA experiment also shows the existence of the first acoustic peak at approximately the same confidence level as Boomerang. But the 1σ contours for the peak position in the plane $(\ell, \ell(\ell+1)C_\ell/2\pi)$ do not intersect. However, their projections onto the ℓ and $\ell(\ell+1)C_\ell/2\pi$ axes do. Approximately one quarter of the area inside the Boomerang 2σ contour falls within the corresponding MAXIMA contour. The same level of agreement of these experiments is found in the data on the 3rd acoustic peak. In the range of 1st dip - 2nd peak - 2nd dip the MAXIMA data give no significant information. Even the 1σ contours are open in both directions of the ℓ axis.

The DASI experiment establishes the location and amplitude of the first acoustic peak at somewhat higher than 1σ C.L. but less than 2σ . The 1σ contours for the position of the first peak of the DASI and Boomerang experiments intersect. Approximately 1/5 of the area outlined by the MAXIMA 2σ contour is within the DASI 2σ contour. The DASI data on second acoustic peak is in excellent agreement with the Boomerang results - the 1σ contours practically coincide.

We have also determined the locations and amplitudes of the acoustic peaks and dips using the data of all three experiments. The results are very close to those from the Boomerang data alone.

To determine cosmological parameters from these data, we have improved the analytical approximations for the peak positions and amplitudes to an accuracy (determined by comparing the approximations with the results of CMBfast) better than 5% in a sufficiently wide range of parameters. We have also developed a fast and accurate analytical method to normalize the power spectrum to the 4-year COBE data on C_{10} . Our analytical approximation is accurate to a few percent (in comparison to CMBfast) when all main effects (ordinary Sachs-Wolfe effect, integrated Sachs-Wolfe effect, adiabatic term, Doppler term and their mutual cross-correlations) are taken into account. For example, in the model with parameters presented in the last row of Table 3 the relation of contribution from these components at $\ell = 10$ are $C_{10}^{\text{SW}} : C_{10}^{\text{A}} : C_{10}^{\text{SW-A}} : C_{10}^{\text{D}} = 1 : 0.098 : -0.24 : 0.42$.

The cosmological parameters extracted from the data on locations and amplitudes of the first

three peaks and the location of the first dip are in good agreement with other determinations (Netterfield et al. 2001; de Bernardis et al. 2001; Pryke et al. 2001; Wang et al. 2001; Durrer & Novosyadlyj 2001). That shows also that present CMB data can essentially be compressed into the height and slope of the Sachs-Wolfe plateau (at $\ell = 10$) and the positions and amplitudes of the first three acoustic peaks and the first two dips.

A remarkable feature is the coincidence of the baryon content obtained from the CMB data, $\Omega_b h^2 \approx 0.02$ with the value from standard nucleosynthesis (0.02 ± 0.001) (Burles et al. 2001). Moreover, the CMB data together with constraints from direct measurements of the Hubble constant, the SNIa data, the baryon content and the large scale structure of the Universe (the power spectrum of rich clusters, the cluster mass function, the peculiar velocity field of galaxies, Ly- α absorption lines as seen in quasar spectra) select a best-fit model which gives predictions within about 1σ error bars of all measurements. The cosmological parameters of this model are $\Omega_\Lambda = 0.64^{+0.14}_{-0.27}$, $\Omega_m = 0.36^{+0.21}_{-0.11}$, $\Omega_b = 0.047^{+0.083}_{-0.024}$, $n_s = 1.0^{+0.59}_{-0.17}$, $h = 0.65^{+0.35}_{-0.27}$ and $\tau_c = 0.15^{+0.95}_{-0.15}$. The best-fit values of Ω_ν and T/S are close to zero, their 1σ upper limits are $\Omega_\nu \leq 0.17$, $T/S \leq 1.7$.

The cosmological parameters determined from the CMB acoustic peak/dip locations and amplitudes data show good agreement with other cosmological measurements and indicate the existence of a simple (adiabatic) best-fit model for all the discussed cosmological data within the accuracy of present experiments.

It is a pleasure to acknowledge stimulating discussions with Alessandro Melchiorri, Roman Juszkiewicz and Roberto Trotta. BN is grateful to the Tomalla foundation for a visiting grant and to Geneva University for hospitality. RD thanks the Institute for Advanced Study for hospitality and acknowledges support from the Monell Foundation.

APPENDIX

A. An analytic approximation for the CMB power spectrum at large angular scales

On sufficiently large angular scales (larger than the Silk damping scale) temperature fluctuations in the CMB can be related to density, velocity and metric perturbations at the last scattering surface and at later times by integrating the geodesic equation, similar to the classical paper by Sachs and Wolfe (1967). Here we discuss only scalar perturbations. Tensor perturbations can be simply added to the result and do not pose any significant difficulty. Scalar perturbations generate CMB temperature fluctuations which can be written in gauge-invariant form as a sum of four terms – the ordinary Sachs-Wolfe effect, the integrated Sachs-Wolfe term, the Doppler term and

the acoustic term (Durrer 1990).

$$\begin{aligned} \left(\frac{\Delta T}{T} \right)^{(s)} (\eta_0, \mathbf{x}_0, \mathbf{n}) = & \frac{1}{4} D_r(\eta_{dec}, \mathbf{x}_{dec}) + V_i(\eta_{dec}, \mathbf{x}_{dec}) n^i + (\Phi - \Psi)(\eta_{dec}, \mathbf{x}_{dec}) \\ & - \int_{\eta_{dec}}^{\eta_0} (\Phi' - \Psi')(\eta, \mathbf{x}(\eta)) d\eta . \end{aligned} \quad (\text{A1})$$

Here Φ and Ψ are the Bardeen potentials (Bardeen 1980), V_i is the baryon velocity and D_r is a gauge invariant variable for the radiation density fluctuations. A prime denotes the partial derivative w.r.t. conformal time η . For perfect fluids and for dust we have $\Psi = -\Phi$. In Newtonian limit the Bardeen potentials just reduce to the ordinary Newtonian potential. For adiabatic perturbations $\frac{1}{4} D_r = \frac{1}{3} \delta_m - \frac{5}{3} \Phi$ (see *e.g.* Durrer & Straumann (1999)), where δ_m is the usual matter density perturbation., it corresponds to ϵ_m in Bardeen's notation. The variables η and \mathbf{x} are conformal time and comoving position.

In realistic models, cosmological recombination and decoupling of radiation from matter take place when $\rho_m > \rho_r$. Hence the large angular scale CMB power spectrum can be expressed in the terms of solutions of Einstein's equations for adiabatic linear perturbations in a dust Universe. The CMB anisotropies on angular scales $\theta \geq 10^\circ$ ($\ell \leq 20$) are generated mainly by the linear perturbations of matter density, velocity and the gravitational potential at scales much larger than the particle horizon at decoupling. Our approximation makes use of these facts.

We use the solutions of Einstein's equations for linear density perturbations in flat models of a Universe with dust and a cosmological constant which can be found in (Kofman & Starobinsky 1985; Apunevych & Novosyadlyj 2000). The growing mode of density, velocity and gravitational potential perturbations, using the gauge-invariant variables introduced by Bardeen (1980) and normalizing the scale factor $a(t_0) = a_0 = 1$, are

$$\Phi(t, k) = K_\delta(t) C(k), \quad \delta_m(t, k) = -\frac{2C(k)k^2 a(t) K_\delta(t)}{3H_0^2 \Omega_m}, \quad V^\alpha(t, k) = -i \frac{2C(k)k^\alpha a(t) \dot{a}(t) K_V(t)}{3H_0^2 \Omega_m}. \quad (\text{A2})$$

$C(k)$ is (up to the time dependent factor K_δ) the Fourier transform of the Bardeen potential, so that $\Phi(t, \mathbf{x}) = (2\pi)^{-3/2} \int \Phi(t, \mathbf{k}) e^{i\mathbf{k}\mathbf{x}} d^3k$, $\delta_m(t, \mathbf{x}) = (2\pi)^{-3/2} \int \delta_m(t, \mathbf{k}) e^{i\mathbf{k}\mathbf{x}} d^3k$ and $V^\alpha(t, \mathbf{x}) = (2\pi)^{-3/2} \int V^\alpha(t, \mathbf{k}) e^{i\mathbf{k}\mathbf{x}} d^3k$. The factors $K_\delta(t) \equiv \frac{5}{3} \left(1 - \dot{a}/a^2 \int_0^t a dt \right)$ and $K_V(t) \equiv \frac{5}{3} \left(\dot{a}/a^2 - \ddot{a}/\dot{a} \right) \int_0^t a dt$ are both in the range $0 < K_\bullet \leq 1$ and reflect the reduction of growth of perturbations caused by the cosmological constant. The scale factor of the background model is given by

$$a(t) = \left(\frac{\Omega_m}{1 - \Omega_m} \right)^{\frac{1}{3}} \sinh^{\frac{2}{3}} \left(\frac{3H_0 t \sqrt{1 - \Omega_m}}{2} \right)$$

Here $H_0 \equiv (\dot{a}/a)(t_0) = \dot{a}(t_0)$ is the Hubble constant today. The K_\bullet -factors go to 1 when $t \ll t_0$ or when $\Omega_m \rightarrow 1$ ($\Omega_\Lambda \rightarrow 0$). At decoupling $K_\delta = K_V = 1$. An analytical approximation for $K_\delta(t)/\Omega_m$ with sufficient accuracy can be found in (Carroll et al. 1992) and for $K_V(t_0)/\Omega_m$ in (Lahav et al. 1991).

The power spectrum of density fluctuations is given by

$$\begin{aligned} P(k, t) &\equiv \langle \delta(t, k) \delta^*(t, k) \rangle = A_s k^{n_s} T_m^2(k; t) a^2(t) K_\delta^2(t) / \Omega_m^2, \\ A_s &= 2\pi^2 \delta_h^2 (3000 \text{Mpc}/h)^{3+n_s}, \end{aligned} \quad (\text{A3})$$

where $T_m(k, t)$ is transfer function (divided by the growth factor) and δ_h is the present matter density perturbation at horizon scale. We use the analytical approximation of $T_m(k, t)$ in the space of cosmological parameters h , Ω_m , Ω_b , Ω_Λ , Ω_ν and N_ν (number of species of massive neutrino) by Eisenstein & Hu (1999).

From Eq. (A1), taking into account adiabaticity and setting $\mathbf{x}_0 = \mathbf{0}$, we obtain

$$\frac{\Delta T}{T}(\mathbf{n}) = \frac{1}{3} \Phi(\eta_{dec}, \mathbf{n}\eta_0) + 2 \int_0^{\omega_e} \frac{\partial \Phi(\eta_0 - \omega, \mathbf{n}\omega)}{\partial \eta} d\omega + n_\alpha V^\alpha(\eta_{dec}, \mathbf{n}\eta_0) + \frac{1}{3} \delta_m(\eta_{dec}, \mathbf{n}\eta_0), \quad (\text{A4})$$

where \mathbf{n} is the unit vector in direction of the incoming photon and we have used $\mathbf{x}(\eta) = \mathbf{n}(\eta_0 - \eta)$, $\mathbf{x}_{dec} \simeq \mathbf{n}\eta_0$. The variable ω is the affine parameter along the geodesic which begins at the observer and ends in the emission point at the last scattering surface. The present value of conformal times, η_0 gives also the present particle horizon or the distance to the last-scattering surface. The first term in (A4) is the well known Sachs-Wolfe effect (SW), the second term is the integrated Sachs-Wolfe effect (ISW) which is important only at late times, where $K_\delta(t)$ starts to deviate from 1 and $\frac{\partial \Phi}{\partial \eta} \neq 0$, the third is the Doppler term (D) and the last is the acoustic term (A). At large angular scales ($\approx 10^\circ$), where anisotropies have been measured by COBE (Bennett et al. 1996), the SW and ISW effects dominate. However, if we want to calculate C_{10} with good accuracy, we must to also take into account the other terms. The angular correlation function of $\Delta T/T$ can be written symbolically as

$$\begin{aligned} \langle \frac{\Delta T}{T}(\mathbf{n}_1) \cdot \frac{\Delta T}{T}(\mathbf{n}_2) \rangle &= \langle \text{SW} \cdot \text{SW} \rangle + 2 \langle \text{SW} \cdot \text{ISW} \rangle + \langle \text{ISW} \cdot \text{ISW} \rangle \\ &\quad + \langle \text{A} \cdot \text{A} \rangle + 2 \langle \text{SW} \cdot \text{A} \rangle + \langle \text{D} \cdot \text{D} \rangle. \end{aligned} \quad (\text{A5})$$

The cross-correlators $\langle \text{D} \cdot \text{SW} \rangle$ and $\langle \text{D} \cdot \text{A} \rangle$ are omitted because they are strongly suppressed on large angular scales. Indeed, if one uses Fourier presentations for the variables (A2) in the equations (A4-A5) one finds that the k -integrand of these terms contains a spherical Bessel function $j_1(k\eta_0(\mathbf{n}_1 - \mathbf{n}_2))$ which oscillates for large angular separations, strongly reducing the integral if compared to the $\langle \text{SW} \cdot \text{A} \rangle$ term where the integrand has a definite sign. The terms $\langle \text{ISW} \cdot \text{A} \rangle$ and $\langle \text{ISW} \cdot \text{D} \rangle$ are also omitted because the ISW effect gives the maximal contribution to $\Delta T/T$ at the largest angular scales of the range of interest (at lowest spherical harmonics) where A and D are nearly zero. At 'smaller' angular scales ($\ell \approx 10$) where contribution of A and D are not negligible, the ISW effect is very small. Therefore, their cross-correlation terms are very small.

We develop the \mathbf{n} -dependence of $\frac{\Delta T}{T}(\mathbf{n})$ in spherical harmonics

$$\frac{\Delta T}{T}(\mathbf{n}) = \sum_{\ell, m} a_{\ell m}(\eta_0) Y_{\ell m}(\mathbf{n}), \quad \langle a_{\ell m} a_{\ell' m'}^* \rangle = \delta_{\ell m} \delta_{\ell' m'} C_\ell.$$

The CMB power spectrum, C_ℓ , has the same components as the correlation function:

$$C_\ell = C_\ell^{\text{SW}} + C_\ell^{\text{SW-ISW}} + C_\ell^{\text{ISW}} + C_\ell^{\text{A}} + C_\ell^{\text{SW-A}} + C_\ell^{\text{D}} \quad (\text{A6})$$

Each component on the right hand side comes from the corresponding contribution to ΔT above and is proportional to δ_h^2 . Using the solutions (A2) we obtain analytic approximations for them.

We first approximate the SW and ISW contributions in the form

$$C_\ell^{\text{SW+ISW}} \equiv C_\ell^{\text{SW}} + C_\ell^{\text{SW-ISW}} + C_\ell^{\text{ISW}} = K_\ell^2 C_\ell^{\text{SW}}, \quad (\text{A7})$$

where the factors K_ℓ (≥ 1) take into account the contribution of the ISW effect for each spherical harmonic. They have been calculated by Kofman & Starobinsky (1985) and Apuneyvych & Novosyadlyi (2000) for different Λ -models. Instead of the direct time consuming calculations of the ISW contribution, we use the following analytic approximations:

$$K_2^2 = 1 + 8.20423 \times \exp(-\Omega_m/0.01157) + 3.75518 \times \exp(-\Omega_m/0.13073),$$

$$K_3^2 = 1 + 2.25571 \times \exp(-\Omega_m/0.03115) + 2.35403 \times \exp(-\Omega_m/0.15805),$$

$$K_4^2 = 1 + 1.80309 \times \exp(-\Omega_m/0.0323) + 1.88325 \times \exp(-\Omega_m/0.16163)$$

$$\text{and } K_\ell^2 = 1 + [23.46523 \times \exp(-\Omega_m/0.0122) + 11.03227 \times \exp(-\Omega_m/0.14558)]/(\ell + 0.5)$$

for $\ell \geq 5$. These approximation formulae are determined from the data presented in the tables of (Kofman & Starobinsky 1985) and (Apuneyvych & Novosyadlyj 2000).

Using solutions (A2) and the definition of the density power spectrum (A4) we obtain the following general expression for the SW contribution to the CMB power spectrum:

$$C_\ell^{\text{SW}} = \frac{\pi \eta_0^{n_s-1} \delta_h^2}{2^{n_s-1} D^2(t_0)} \int_0^\infty dk k^{n_s-2} T_m^2(t_{\text{dec}}, k) j_\ell^2(k\eta_0), \quad (\text{A8})$$

where $T_m^2(t_{\text{dec}}, k)$ is the transfer function of matter density perturbations at decoupling, $D(t_0) \equiv K_\delta(t_0)/\Omega_m$ is the value of the growth factor at the current epoch, and j_ℓ is the spherical Bessel function of order ℓ . For reasonable values of spectral index $-3 \leq n_s \leq 3$ the main contribution to the integral (A8) comes from very small k where $T_m(t_{\text{dec}}, k) \approx 1$ and can be omitted. Then integral can be performed analytically and the result can be expressed in terms of Γ -functions:

$$C_\ell^{\text{SW}} = \frac{\pi^2 \delta_h^2}{8 D^2(t_0)} \frac{\Gamma(3 - n_s) \Gamma(\ell + \frac{n_s-1}{2})}{\Gamma^2(2 - n_s/2) \Gamma(\ell + \frac{5-n_s}{2})}. \quad (\text{A9})$$

In the same way we obtain the expressions for the other components of equation (A6):

$$C_\ell^{\text{A}} = \frac{\pi \eta_0^{n_s+3} \delta_h^2 a^2(t_{\text{dec}})}{18 \cdot 2^{n_s} D^2(t_0) \Omega_m^2} \int_0^\infty dk k^{n_s+2} T_b^2(t_{\text{dec}}, k) j_\ell^2(k\eta_0), \quad (\text{A10})$$

$$C_\ell^{\text{SW-A}} = -\frac{\pi \eta_0^{n_s+1} \delta_h^2 a(t_{\text{dec}})}{3 \cdot 2^{n_s-1} D^2(t_0) \Omega_m} \int_0^\infty dk k^{n_s} T_m(t_{\text{dec}}, k) T_b(t_{\text{dec}}, k) j_\ell^2(k\eta_0), \quad (\text{A11})$$

$$C_\ell^{\text{D}} = \frac{\pi \eta_0^{n_s+1} \delta_h^2 a(t_{\text{dec}})}{2^{n_s-1} D^2(t_0) \Omega_m} \int_0^\infty dk k^{n_s} T_b^2(t_{\text{dec}}, k) j_\ell'^2(k\eta_0),, \quad (\text{A12})$$

where $T_b(t_{dec})$ is transfer function for density perturbations of baryons (Eisenstein & Hu 1998) and $(')$ is the derivative w.r.t the argument $x = k\eta_0$. The minus sign in the expression for $C_\ell^{\text{SW-A}}$ reflects the anti-correlation of the gravitational potential and density fluctuations: large positive density fluctuations generate deep negative potential wells. If we set $T_m = T_b = 1$, the integrals (A11 –A12) diverge for all ℓ for $n_s \geq 1$ because the main contribution to integrals of the D and A terms comes from small scales. Hence here the transfer functions must be kept and the integrals have to be calculated numerically. Fortunately, the integrands decay rapidly for large wave numbers and 99.9% of the contribution comes from the range $0.001 \leq k\eta_{dec} \leq 0.1$, so that the integration is not very time consuming.

In Fig.7 the CMB power spectrum C_ℓ at large angular scales ($\theta \geq 20^\circ$, $\ell \leq 20$) together with the contributions from the different terms given in (A9-A12) is shown for a pure matter and a Λ –dominated model. The relation of the contributions from different terms at $\ell = 10$ are

$$C_\ell^{\text{SW}} : C_\ell^{\text{A}} : C_\ell^{\text{SW-A}} : C_\ell^{\text{D}} = 1 : 0.04 : -0.11 : 0.22$$

for the matter dominated flat model ($\Omega_m = 1$) and

$$C_\ell^{\text{SW}} : C_\ell^{\text{A}} : C_\ell^{\text{SW-A}} : C_\ell^{\text{D}} = 1 : 0.08 : -0.23 : 0.39.$$

for the Λ dominated model with the cosmological parameters shown in the figure. Therefore, a few percent accuracy of the normalization to 4-year COBE C_{10} data can be achieved only if all these effects are taken into account.

In Fig. 8 the CMB power spectrum at large scales calculated using the analytic formulae (A9-A12) and using CMBfast are shown for comparison. In the left panel we also present the power spectrum calculated by the analytical approach of (Hu & Sugiyama 1995) (renormalized to the CMBfast value of C_{10}).

The calculations show that value of C_{10} calculated by our method deviates from the value calculated with CMBfast by 0.5% for the matter dominated flat model ($\Omega_m = 1$) and 2.7% for the Λ dominated model ($\Omega_m = 0.2$). Therefore, our analytic approach is sufficient to normalize fast the power spectrum of scalar perturbations to the 4-year COBE data with virtually the same precision as CMBfast, the difference is less than 3%. (Remember, that the experimental errors of the COBE data are about 14%, so that the best-fit normalization parameter C_{10}^{COBE} has the same error.)

Another comparison of our normalization procedure with CMBfast comes from the value of σ_8 . For the flat model (left panel of Fig. 8) our approximation for the normalization together with the analytical transfer function of Eisenstein & Hu (1998; 1999) leads to $\sigma_8 = 1.58$, the corresponding value calculated from CMBfast is 1.53. For the Λ dark matter model (right panel) our $\sigma_8 = 0.62$, while CMBfast gives $\sigma_8 = 0.64$. The agreement of both approaches is quite well (the 5% difference includes also the errors in the approximation of the transfer function which is actually of this order).

The slight deviation of C_{10} as calculated by our code from the value obtained with CMBfast ($\leq 3\%$) in spite of using the same analytic best-fit formula for C_{10}^{COBE} by (Bunn & White 1997)

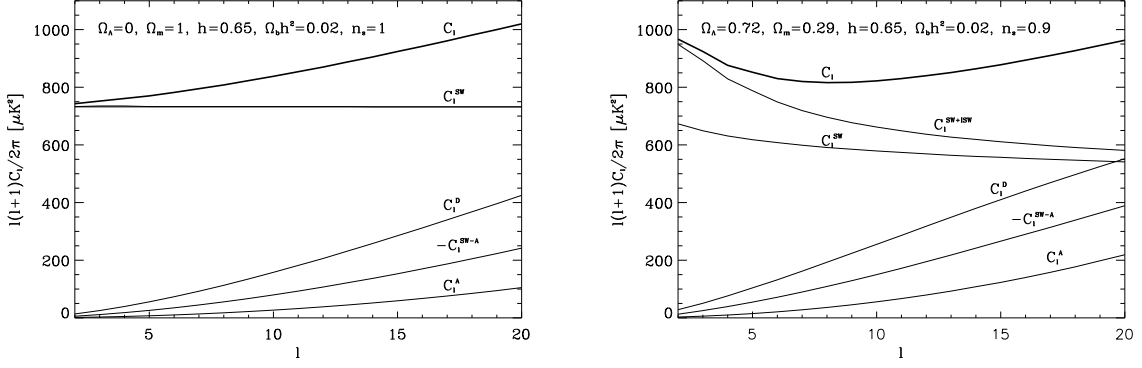


Fig. 7.— The CMB power spectrum and the different contributions discussed in the text (formulae A9-A12) for a pure matter model (left panel) and a Λ dominated model (right panel).

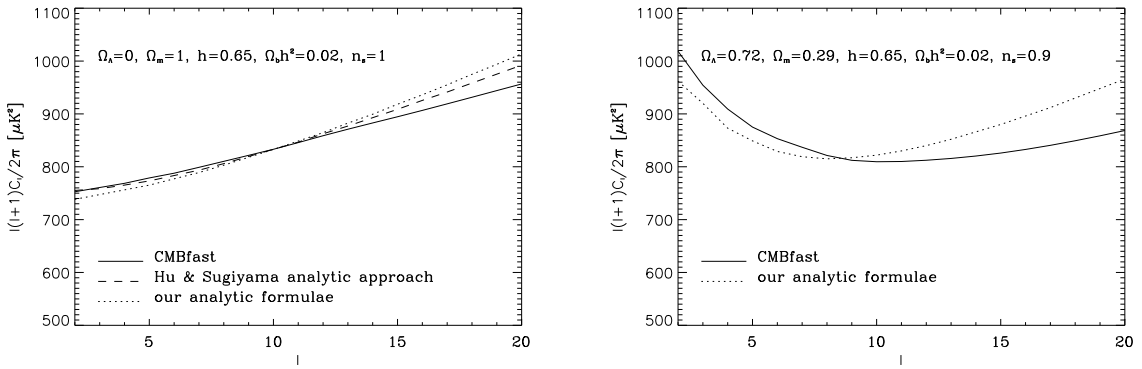


Fig. 8.— The CMB power spectrum at COBE scales calculated by CMBfast (solid line) and by our analytical formulae (A9-A12) (dotted line). For the pure matter model we also show the spectrum calculated with the analytic approach of (Hu & Sugiyama 1995) (dashed line) (this approach does not allow a cosmological constant). All spectra are normalized to the best fit for C_{10} from the 4-year COBE data given in (Bunn & White 1997).

is due to a difference in the form of the spectra as shown in the Fig. 8. This difference grows when Ω_m decreases. There are several possible reasons for this deviation in the form of the CMB power spectrum in our analytic approach from the exact numerical calculation: 1) We have used the solutions for the evolution of density, velocity and gravitational potential perturbations in the Λ -dust Universe. In reality, at decoupling the role of radiation is not completely negligible, this slightly influences the dynamics of the scale factor and the evolution of perturbations. It also results in additional time dependence of gravitational potential (early integrated Sachs-Wolfe effect) which is not taken into account here. 2) Our approach does not take into account the effects of the collisionless dynamics of photons and neutrinos after decoupling. Especially, the induced anisotropic stresses lead to $\approx 10\%$ difference of the gravitational potentials in the radiation-dominated epoch which results into a corrections of a few percent in the C_ℓ 's. 3) Instantaneous recombination and tight coupling which were assumed, also cause slight inaccuracies. They should, however, be extremely small on the angular scales considered here. 4) To calculate the terms C_ℓ^A , C_ℓ^{SW-A} and C_ℓ^D we have used the analytic approximations for the transfer functions, $T_m(t_{dec}, k)$ and $T_b(t_{dec}, k)$, by Eisenstein & Hu (1998; 1999) which have an accuracy $\sim 5\%$.

More details on the theory of CMB anisotropies can be found in the reviews by Durrer & Straumann (1999) and Durrer (2001).

B. Analytic formulae for the amplitudes and locations of acoustic peaks and dips in the CMB power spectrum

For completeness, we repeat here the formulas used in our parameter search which can also be found in the cited literature.

We assume the standard recombination history and define the redshift of decoupling z_{dec} as the redshift at which the optical depth of Thompson scattering is unity. A useful fitting formula for z_{dec} is given by (Hu & Sugiyama 1996):

$$z_{dec} = 1048[1 + 0.00124\omega_b^{-0.738}][1 + g_1\omega_m^{g_2}], \quad (\text{B1})$$

where

$$g_1 = 0.0783\omega_b^{-0.238}[1 + 39.5\omega_b^{0.763}]^{-1}, \quad g_2 = 0.56[1 + 21.1\omega_b^{1.81}]^{-1},$$

$\omega_b \equiv \Omega_b h^2$ and $\omega_m \equiv \Omega_m h^2$.

B.1. Locations

The locations of the acoustic peaks in the CMB power spectrum depend on the value of sound horizon at decoupling epoch $r_s(\eta_{dec}) \equiv \int_0^{\eta_{dec}} d\eta' c_s$ and the angular diameter distance to the last scattering surface, $d_A(z_{dec})$. Comparing with numerical calculations it was shown (see (Efstathiou & Bond 1999; Hu et al. 2001; Doran & Lilley 2001) and references therein) that the spherical harmonic which corresponds to the m -th acoustic peak is well approximated by the relation

$$\ell_{p_m} = (m - \phi_m)\pi \frac{d_A(z_{dec})}{r_s(z_{dec})}, \quad (\text{B2})$$

where ϕ_m take into account the shift of m -th peak from its location in the idealized model which is caused by driving effects from the decay of the gravitational potential. Doran and Lilley (2001) give an accurate analytic approximation in the form

$$\phi_m = \bar{\phi} - \delta\phi_m, \quad (\text{B3})$$

where $\bar{\phi}$ is overall phase shift of the spectrum (or the first peak) and $\delta\phi_m$ is a relative shift of each peak and dip caused by the Doppler shift of the oscillating fluid. For the overall phase shift of the spectrum they find

$$\bar{\phi} = (1.466 - 0.466n_s)a_1 r_*^{a_2}, \quad (\text{B4})$$

where

$$r_* \equiv \rho_{rad}(z_{dec})/\rho_m(z_{dec}) = \frac{0.0416}{\omega_m} \left(\frac{1 + \rho_\nu/\rho_\gamma}{1.6813} \right) \left(\frac{T_0}{2.726} \right)^4 \left(\frac{z_{dec}}{1000} \right)$$

is the ratio of radiation to matter at decoupling, and

$$a_1 = 0.286 + 0.626\omega_b, \quad a_2 = 0.1786 - 6.308\omega_b + 174.9\omega_b^2 - 1168\omega_b^3$$

are fitting coefficients. Here and below the numbers in the expressions are obtained for a present CMB temperature of $T_0 = 2.726\text{K}$ and the ratio of densities of massless neutrinos and photons $\rho_\nu/\rho_\gamma = 0.6813$ for three massless neutrino species (correspondingly $f_\nu \equiv \rho_\nu/(\rho_\gamma + \rho_\nu) = 0.405$). All values can be easily scaled to other values of T_0 and f_ν .

The relative shift of the 1st acoustic peak is zero, $\delta\phi_1 = 0$. For the 2nd one it is

$$\delta\phi_2 = c_0 - c_1 r_* - c_2/r_*^{c_3} + 0.05(n_s - 1) , \quad (\text{B5})$$

with

$$c_0 = -0.1 + 0.213e^{-52\omega_b}, \quad c_1 = 0.015 + 0.063e^{-3500\omega_b^2}, \quad c_2 = 6 \cdot 10^{-6} + 0.137(\omega_b - 0.07)^2, \quad c_3 = 0.8 + 70\omega_b,$$

and for the 3rd peak

$$\delta\phi_3 = 10 - d_1 r_*^{d_2} + 0.08(n_s - 1) , \quad (\text{B6})$$

with

$$d_1 = 9.97 + 3.3\omega_b, \quad d_2 = 0.0016 + 0.196\omega_b + 2.25 \cdot 10^{-5}\omega_b^{-1}.$$

The formula (B2) is correct also for the location of dips if we set $m = 3/2$ for the 1st dip and $m = 5/2$ for the 2nd dip. The relative shift of the first dip given by (Doran & Lilley 2001) is

$$\delta\phi_{3/2} = b_0 + b_1 r_*^{1/3} \exp b_2 r_* + 0.158(n_s - 1) \quad (\text{B7})$$

with

$$b_0 = -0.086 - 2.22\omega_b - 140\omega_b^2, \quad b_1 = 0.39 - 18.1\omega_b + 440\omega_b^2, \quad b_2 = -0.57 - 3.8 \exp(-2365\omega_b^2) .$$

The angular diameter distance to the last scattering surface is given by

$$d_A(z_{dec}) = \frac{c}{H_0 \sqrt{|\Omega_k|}} \chi(\eta_0 - \eta_{dec}) , \quad (\text{B8})$$

where $\chi(x) = x$, $\sin x$ or $\sinh x$ for flat, closed or open models respectively, and

$$\eta_0 - \eta_{dec} = \sqrt{|\Omega_k|} \int_0^{z_{dec}} \frac{dz}{\sqrt{\Omega_{rad}(z+1)^4 + \Omega_m(z+1)^3 + \Omega_\Lambda + \Omega_k(z+1)^2}} . \quad (\text{B9})$$

Since, the sound speed in the pre-recombination plasma is

$$c_s = c/\sqrt{3(1+R)} \quad \text{with} \quad R \equiv 3\rho_b/4\rho_\gamma = 30315(T_0/2.726)^{-4}\omega_b a \quad (\text{B10})$$

and scale factor is well approximated by

$$a(\eta) = a_{eq} \left(\frac{\eta}{\eta_1} + \left(\frac{\eta}{2\eta_1} \right)^2 \right) , \quad (\text{B11})$$

with

$$a_{eq} = \frac{4.16 \cdot 10^{-5}}{\omega_m} \left(\frac{1 + \rho_\nu / \rho_\gamma}{1.6813} \right) \left(\frac{T_0}{2.726} \right)^4, \quad \eta_1 \equiv \frac{\eta_{eq}}{2(\sqrt{2} - 1)},$$

the integral for sound horizon can be reduced to the analytic formula

$$r_s(\eta_{dec}) = \frac{19.9}{\sqrt{\omega_b \omega_m}} \left(\frac{T_0}{2.726} \right)^2 \ln \frac{\sqrt{1 + R_{dec}} + \sqrt{R_{dec} + R_{eq}}}{1 + \sqrt{R_{eq}}} \text{ Mpc.} \quad (\text{B12})$$

The deviation of the acoustic extrema locations calculated using formulae (B2-B12) from the values obtained by CMBfast code is < 3% for a sufficiently wide range of parameters.

B.2. Amplitudes

The amplitude of the 1st acoustic peak can be approximated by the following expression

$$A_{p_1} = \frac{\ell_{p_1}(\ell_{p_1} + 1)}{2\pi} \left[C_{\ell_{p_1}}^{SW} + C_2^{SW} \tilde{\mathcal{A}}(\Omega_b, \Omega_{cdm}, \Omega_k, n_s, h) \right], \quad (\text{B13})$$

where

$$\tilde{\mathcal{A}} \equiv 0.838 \mathcal{A} = \exp [\tilde{a}_1 + a_2 \omega_{cdm}^2 + a_3 \omega_{cdm} + a_4 \omega_b^2 + a_5 \omega_b + a_6 \omega_b \omega_{cdm} + a_7 \omega_k + a_8 \omega_k^2 + a_9 (n_s - 1)] \quad (\text{B14})$$

and $C_{\ell_{p_1}}^{SW}$ is given by (A9). We have re-determined the best-fit coefficients a_i using the values of the 1st acoustic peak amplitudes from CMBfast for the grid of parameters given below. Their values are

$$\begin{aligned} \tilde{a}_1 &= 2.326, \quad a_2 = 8.906, \quad a_3 = -7.733, \quad a_4 = -115.6, \quad a_5 = 35.66, \\ a_6 &= -7.225, \quad a_7 = 1.96, \quad a_8 = -11.16, \quad a_9 = 4.439. \end{aligned} \quad (\text{B15})$$

The deviations of this approximation from the numerical value obtained by CMBfast are $\leq 5\%$ within the range of cosmic parameters, $0.2 \leq \Omega_m \leq 1.2$, $0 \leq \Omega_\Lambda \leq 0.8$, $0.015 \leq \Omega_b \leq 0.12$, $0.8 \leq n_s \leq 1.2$ and $0.4 \leq h \leq 1.0$.

To calculate the amplitudes of the 2nd and 3rd peaks we use the relations

$$H_2 \equiv \left[\ell_{p_2}(\ell_{p_2} + 1) C_{\ell_{p_2}} \right] / \left[\ell_{p_1}(\ell_{p_1} + 1) C_{\ell_{p_1}} \right] \quad \text{and} \quad H_3 \equiv \left[\ell_{p_3}(\ell_{p_3} + 1) C_{\ell_{p_3}} \right] / \left[\ell_{p_1}(\ell_{p_1} + 1) C_{\ell_{p_1}} \right]$$

given by Hu et al. (2001). This leads to the following amplitudes

$$A_{p_2} = A_{p_1} H_2(\Omega_m, \Omega_b, n_s), \quad \text{with} \quad H_2 = \frac{0.925 \omega_m^{0.18} 2.4^{n_s - 1}}{\left[1 + (\omega_b / 0.0164)^{12 \omega_m^{0.52}} \right]^{1/5}}, \quad (\text{B16})$$

$$A_{p_3} = A_{p_1} H_3(\Omega_m, \Omega_b, n_s), \quad \text{with} \quad H_3 = \frac{2.17 \omega_m^{0.59} 3.6^{n_s - 1}}{\left[1 + (\omega_b / 0.044)^2 \right] \left[1 + 1.63(1 - \omega_b / 0.071) \omega_m \right]}. \quad (\text{B17})$$

This approximation for A_{p_3} deviates by less than 5% from the value obtained with CMBfast for parameters within the range specified above. The accuracy of A_{p_2} is better than 9%. For some parameter values the second peak is under estimated leading to this somewhat poorer accuracy.

REFERENCES

- Apunevych, S. & Novosyadlyj, B., 2000, Journal of Physical Studies, 4, 470
- Bahcall, N.A. & Fan, X., 1998, ApJ, 504, 1
- Balbi, A. et al., 2000, ApJ, 545, L1
- Bardeen, M., 1980, Phys. Rev., D22, 1882
- Bennett, C.L. et al., 1996, ApJ, 464, L1
- de Bernardis, P. et al., 2000, Nature, 404, 495
- de Bernardis, P. et al., 2001, astro-ph/0105296
- Burles, S. Nollet, K.M and Turner, M.S., 2001, Astrophys. J. Lett. **552**, L1–L6
- Bunn, E.F. & White, M., 1997, ApJ, 480, 6
- Carroll, S.M., Press, W.H. and Turner, E.L., 1992, ARA&A, 30, 499
- Doran, M. & Lilley, M., 2002, MNRAS, 330, 965
- Douspis, M. & Ferreira, P.G., 2001, astro-ph/0111400
- Durrer, R., 1990, Phys. Rev. D42, 2533
- Durrer, R., 2001, astro-ph/0109522; 2001, Journal of Physical Studies, 5, No 2, 177
- Durrer, R. & Novosyadlyj, B., 2001, MNRAS, 324, 560
- Durrer, R. & Straumann, N., 1999, *New methods for the determination of cosmological parameters.* Troisième Cycle de la Physique en Suisse Romande, Université de Lausanne.
- Efstathiou, G. & Bond, J.R., 1999, MNRAS, 304, 75
- Eisenstein, D.J. & Hu, W., 1998, ApJ, 496, 605
- Eisenstein, D.J. & Hu, W., 1999, ApJ, 511, 5
- Gorski, K. M. et al., 1996, ApJ, 464, L11
- Halverson, N.W. et al., 2001, astro-ph/0104489

- Hanany, S. et al., 2000, ApJ, 545, L5
- Hu, W., Fukugita, M., Zaldarriaga, M. and Tegmark, M., 2001, ApJ, 549, 669
- Hu, W. & Sugiyama, N., 1995, ApJ, 444, 489
- Hu, W. & Sugiyama, N., 1996, ApJ, 471, 542
- Hu, W. & White, M., 1996, ApJ, 471, 30
- Kofman, L. & Starobinsky, A.A., 1985, Sov. Astron. Lett., 11(5), 271
- Knox, L. & Page, L., 2000, Phys. Rev. Lett., 85, 1366
- Lahav, O., Lilje, P.B., Primack, J. and Rees, M.J., 1991, MNRAS, 251, 128
- Lange, A.E. et al., 2001, Phys. Rev. D63, 042001
- Lee, A.T. et al., 2001, astro-ph/0104459
- Miller, C.J. & Nichol, R.C., 2001, astro-ph/0112049
- Netterfield, C.B. et al., 2001, astro-ph/0104460
- Novosyadlyj, B., Durrer, R. and Lukash, V.N., 1999, A&A, 347, 799
- Novosyadlyj, B., Durrer, R., Gottloeber, S., Lukash, V.N. and Apunevych, S., 2000, A&A, 356, 418
- Perlmutter, S. et al., 1999, ApJ517, 565
- Pryke, C. et al., 2001, astro-ph/0104490
- Sachs, R.K. & Wolfe, A.M., 1967, ApJ, 147, 73
- SDSS Collaboration: Szalay, A.S. et al., 2001, astro-ph/0107419
- Seljak, U. & Zaldarriaga M., 1996, ApJ 469, 437
- Smoot, G.F et al. 1992, ApJ **396**, L1
- Tegmark, M., Zaldarriaga, M. & Hamilton, A.J.S., 2001, Phys. Rev. D63, 43007
- Wang, X., Tegmark, M. & Zaldarriaga, M., 2001, astro-ph/0105091